MULTIPHYSICS NUMERICAL MODEL FOR PFAS TRANSPORT WITHIN

VADOSE AND SATURATED ZONES

by

Pierrette Iradukunda

A thesis

submitted in partial fulfillment

of the requirements for the degree of

Master of Science in Civil Engineering

Boise State University

August 2023

BOISE STATE UNIVERSITY GRADUATE COLLEGE

DEFENSE COMMITTEE AND FINAL READING APPROVALS

of the thesis submitted by

Pierrette Iradukunda

Thesis Title: Multiphysics Numerical Modeling for PFAS Transport within Vadose and Saturated Zones

Date of Final Oral Examination: January 4th, 2023

The following individuals read and discussed the thesis submitted by student Pierrette Iradukunda, and they evaluated the student's presentation and response to questions during the final oral examination. They found that the student passed the final oral examination.

Arvin Farid, Ph.D.   Chair, Supervisory Committee

Kevin Roche, Ph.D.   Member, Supervisory Committee

Jodi Mead, Ph.D.   Member, Supervisory Committee

The final reading approval of the thesis was granted by Arvin Farid, Ph.D., Chair of the Supervisory Committee. The thesis was approved by the Graduate College.

DEDICATION

I dedicate this work to my family and friends whose support meant a lot to me during this journey. I am forever grateful to my husband, Yannick, for his encouragement and support.

ACKNOWLEDGMENTS

ABSTRACT

The extent and severity of wildfires have increased around the world, necessitating a greater understanding of the consequences of wildfire and post-fire impacts on soil and groundwater. Wildfire suppression techniques like aqueous film-forming foams (AFFF) can also contaminate the soil with per- and polyfluoroalkyl substances (PFAS), which can contribute to human and environmental health concerns. PFAS are dangerous man-made chemical compounds that are persistent, mobile, poisonous, and a major cause of soil and groundwater contamination. In addition to contamination by aqueous film-forming foams, PFAS has accumulated in the environment as a result of being utilized in numerous other goods over time. PFAS are popular because of a number of physiochemical characteristics that make them beneficial in a range of products and industries, furthering their spread. There are several uncertainties about the fate and transport of PFAS in unsaturated zones, as well as how the subsurface groundwater is impacted. This is because of PFAS's tendency for biotransformation, bioaccumulation, and partitioning, as well as persistence in the environment due to their robust C-F bond. Therefore, concerns are raised about their fate, transport, and adverse impacts on the ecosystem, people, and other biota. In this research, the fate and transport of PFAS (specifically Perfluorooctane Sulfonic acid, PFOS) in both saturated and unsaturated zones are investigated through numerical modeling using the finite-difference method.

This study investigates the effect of various transport processes (advection, diffusion, and adsorption) on the fate of PFAS in soil and groundwater. The numerical model is developed to simulate the transport of PFAS in the vadose and saturated soils. After development, the sensitivity of the model results to the spatial and temporal discretization (i.e., selection of time, dt, and space, dz) resolution was analyzed. The results demonstrate very low (less than 2%) sensitivity to dt in the range of 2 to 20 seconds (actually tested at 2, 5, 10, and 20 seconds) and to dz in the range of 0.001 to 0.02 m. (actually tested at 0.001, 0.0025, 0.005, 0.0075, and 0.01 m), respectively. To qualitatively test and verify the model and comprehend the fate and mobility of PFAS in both vadose and saturated zones, a number of scenarios were then explored using the model.

TABLE OF CONTENTS

LIST OF TABLES

LIST OF FIGURES

LIST OF ABBREVIATIONS

1D   One dimensional

AEC   Anion Exchange Capacity

AFFF   Aqueous Film-Forming Foams

CEC   Cation Exchange Capacity

C-F   Carbon-Fluoride

FDM   Finite-Difference Method

FTS   Fluorotelomer Sulfonate

OC   Organic Carbon

PDE   Partial Differential Equations

PFAA   Perfluoroalkyl Acid

PFAS   Per- and Polyfluoroalkyl substances

PFOA   Perfluorooctanoic Acid

PFOS   Perfluorooctane Sulfonic Acid

CHAPTER ONE: INTRODUCTION

Aside from the direct impact on human lives and health, wildfires can have a variety of direct and indirect effects on soil and its ecosystems. As wildfire seasons and regions across the United States and the world expand, so does the need to understand the effects of wildfires on soil, including their contaminating effects. Both wildfires and fire suppression have negative environmental consequences. Wildfires can be put out with the help of a popular and efficient firefighting method using aqueous film-forming foams (AFFF). AFFF is a foaming agent and fluorinated surfactant blend. These fluorinated surfactants' active main ingredients can be categorized as per- and polyfluoroalkyl substances (PFAS). PFAS are synthetically manufactured fluorinated organic compounds (Barzen-Hanson et al., 2017; Wang et al., 2017). In addition to their use in firefighting foams, PFAS has been used in a variety of industrial and commercial products such as nonstick coatings, carpets and textiles, and paper products. Because of its unique properties, such as water repellency and fire and chemical stability—due to the strong Carbon and Fluorine (C-F) covalent bond—PFAS is widely used in several products. These characteristics are useful in both consumer and industrial products. However, the same properties of PFAS contribute to soil and aquifer contamination, due to PFAS discharge into the environment since the 1940s. Perfluorooctane sulfonic acid (PFOS), perfluorooctanoic acid (PFOA), and a variety of other chemicals are found commonly in sediments and groundwater, having been linked to placental and fetal abnormalities (Blake& Fenton, 2020; Nian et al., 2020), altering baby growth (Liew et al., 2018),

cancer (Viera et al., 2013), and many other health hazards (Xu et al., 2020; Steenland et al., 2020). PFAS can contaminate drinking water through a variety of scenarios, including accumulation, leaching due to rainfall, environmental, and leaching from the use of AFFF-based firefighting foams. Predicting PFAS' unidentified environmental risks and hazards requires a better understanding of their fate and behavior. Hence, this study focuses on the understanding of the fate and transport of PFAS in vadose and saturated zones with the geoenvironment using numerical modeling.

The main goal of this research is to understand the fate and transport of PFAS through the vadose zone and groundwater via numerical modeling. A numerical model will be developed to simulate and examine seepage (flow of water) through both saturated and unsaturated soils. Then the seepage model will be coupled with another code developed to simulate the PFAS transport in those zones. The Hypothesis of this research is that the PFAS transport can be numerically modeled considering advection, dispersion and adsorption and that the results will be consistent with experimental results from literature. This study uses physics presented in Guo et al. (2020). However, a different approach was applied to resolve the degree of saturation S_w and well as the volumetric water content, θ where a modified Iterated Crank-Nicolson Method was used. In addition, the MATLAB code created in this thesis is set up to accommodate for addition physics and processes in the future such as chemical or biological transformation.

This thesis consists of an introduction in Chapter One, three manuscripts in Chapters 2, 3, and 4, and a summary of conclusions in Chapter 5. The three manuscripts are interrelated. Chapter two consists of an overall introduction to the work being

presented in this thesis. Chapter three is the first manuscript, "post-wildfire soil and aquifer contamination: A review," published in the Coupled Phenomena in Environmental Geotechnics (CPEG) 2020 conference in Japan. This is a review paper about the existing literature on PFAS, its fate and transport, and identification of the areas of research need. Chapter three is the second manuscript, "Multiphysics numerical modeling of transient transport of PFAS," a conference paper published in GeoCongress 2022. This chapter details the background and literature review of PFAS and its transport in the environment. Chapter four is the final manuscript, "Effects of adsorption coefficients on PFAS transport through vadose and saturated zones using a 1D finite-difference model," a manuscript that has been submitted to the Journal of Contaminant Hydrology. This chapter is a continuation of the second manuscript and focusses on the methodology and results from the numerical model discussed in the second manuscript. Lastly, Chapter five is an overall conclusion and suggestions for further improvement and expansion of this model. The appendices will present the derivations of the seepage and transport equations as well as the scripts of codes developed using the MATLAB interface.

CHAPTER TWO: POST-WILDFIRE SOIL AND AQUIFER CONTAMINATION: A

REVIEW

2.1 Abstract

The need to understand the effects of wildfire and post-fire contamination of soil

and groundwater has grown as a result of the expansion of the extent and severity of

wildfires around the world. In addition to their direct hazards, wildfires can also

contribute to human and environmental health concerns due to secondary contamination,

e.g., wildfire suppression such as aqueous film-forming foams (AFFF) can release per-

and polyfluoroalkyl substances (PFAS, very mobile, toxic, and persistent substances) into

the soil. Both direct seepage through the topsoil and biotransformation of fluorotelomers

(FTs) determine the fate of PFAS in soils and aquifers. Research has indicated that phase

partitioning behavior, such as sorption to soils and sediments, controls the fate and

transport of chemicals in the environment According to various studies, the main soil or

sediment characteristics that control PFAS' sorption behavior include organic carbon

(OC), pH, index cations, and ionic strength. However, neither OC, pH, nor clay-content

alone could explain the sorption behavior of PFAS. More research is needed to help to

understand the role of co-contaminants on the sorption behavior of PFAS, the role of

surface charge on the sorption of PFAS, and on a wider range of PFAS chain compounds

in the future. This paper aims to review the fate and transport of PFAS and identify the

areas of research need.

2.2 introduction

In addition to the direct impact of wildfires on human lives and health, wildfires

can leave various direct and indirect impacts on soil and its ecosystem. The need to

understand the effects of wildfire on soil, including its contaminating effect, is growing

as a result of expanding wildfire seasons and regions across the U.S. and the globe. Fire

and fire suppression after wildfires both result in harmful impacts on the environment.

The use of aqueous film-forming foam (AFFF) is a popular and effective firefighting

method to suppress wildfires. AFFF is a mix of foaming agents and fluorinated

surfactants. Per- and Polyfluoroalkyl substances (PFAS) are the active ingredients in

these fluorinated surfactants. PFAS consists of a broad group of perfluoroalkyl and

polyfluoroalkyl substances. This group contains diverse categories and classes unified by

the presence of a perfluoroalkyl group but differing in ionic, cationic, and zwitterionic

species (Barzen-Hanson et al., 2017). These compounds have notable uses such as

imparting oil, water repellency in consumer products, and reducing surface tension in

firefighting foams (Houtz et al., 2016). The polyfluorinated compounds in AFFF and

their polyfluorinated intermediated products are known as perfluoroalkyl acid (PFAA)

precursors, also referred to simply as precursors. Figure 2.1 shows two 8-carbon (C8)

types of PFAS, Perfluorooctane sulfonate (PFOS) and perfluorooctanoate (PFOA), the

most manufactured and investigated PFAA compounds (Houtz et al., 2016). PFAS

typically have a carbon-fluorine tail and a nonfluorinated head consisting of a polar

functional group. The tail is hence hydrophobic while the head is polar and hydrophilic

(ITRC, 2018).

Perfluorooctane Sulfonate (PFOS)

Tail $F_3C\text{-}CF_2\text{-}CF_2\text{-}CF_2\text{-}CF_2\text{-}CF_2\text{-}CF_2\text{-}CF_2$ SO_3^- Head

Perfluorooctane Carboxylate (PFOA)

Tail $F_3C\text{-}CF_2\text{-}CF_2\text{-}CF_2\text{-}CF_2\text{-}CF_2\text{-}CF_2\text{-}CF_2$ CO_2^- Head
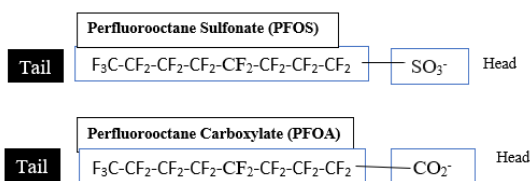
Fig. 2.1. The tail and head structure of PFOS and PFOA molecules (adapted from a figure by ITRC, 2018).

PFAS contributes to the contamination of the soil and aquifers and has been released into the environment for over 50 years (Houde et al. 2011). PFAS, including perfluorooctane sulfonic acid (PFOS), perfluorooctanoic acid (PFOA), and many other chemicals, are usually detectable in sediment and groundwater media. Because PFAS are very stable, they have been utilized in many products. Nowadays, scientists pay more attention to PFAS and their fate in and effects on the environment. This is due to PFAS' resistance to degeneration, their bioaccumulation properties, and toxicity and hazard for humans and living organisms (Martin et al., 2003). Several studies have shown that PFAS can pollute soil, sediments, and surface- and groundwater during the use of firefighting AFFFs (Backe et al., 2013; Munoz et al., 2017), but it is obvious that data and research about the fate and transport of PFAS are not, by any means, complete and still require more research. PFAS can be released into the environment through direct (their formation cycle) and indirect (alteration of their precursors) sources, i.e., they have point (industrial sites) and nonpoint sources (Buck et al., 2011). The fate of PFAS consists of their partitioning, transport (advection, dispersion, and diffusion), and transformation. Various partitioning processes have a significant role in determining and understanding the PFAS transport. Because of the heterogeneity of the subsurface environment, understanding the fate and transport of PFAS requires consideration of several partitioning mechanisms. PFAS have surfactant properties, which make them different from other contaminants (Oliver et al., 2013), making the prediction of their behavior in the soil difficult (Baduel et al., 2017). Most research on the fate and behavior of PFAS in the environment has focused on the transport, remediation, and source of these contaminations on a small fraction (PFOS and PFAS) of these compounds (Miyake et al., 2007). Xiao (2017)

reviewed recent research focused on the fate and behavior, existence, and identification of novel PFAS in groundwater. Xiao (2017) concluded that studies regarding the fate of novel PFAS in rivers, aquifers, drinking water, and during treatment are very limited. Barzen-Hanson et al. (2017) focused on the sorption of anionic, cationic, and zwitterionic novel PFAS, which exist in AFFF. They showed that the sorption of cationic and zwitterionic compounds, due to both hydrophobic and electrostatic behavior, and the sorption of anionic substances that are controlled by hydrophobic interaction are very complex and impossible to be predicted by soil characteristic. Mejia-Avendaño et al. (2020) also claimed that the fate and transport of cationic and zwitterionic compounds are not well understood.

Understanding the fate and behavior of novel PFAS can help to predict their unknown environmental risks and dangers. This paper briefly reviews the research on the fate and transport of novel PFAS released into the environment.

2.3 Flow and Transformation Mechanisms of PFAS

Dauchy et al. (2019) attempted to determine the depth to which PFAS can penetrate the soil. They evaluated the seepage of four classes of PFAS into the soil (PFSA, PFCA, PFOS precursors, and FTS. The results and observations of other studies confirmed that it is difficult to determine the fate of PFAS in soil and groundwater because it depends on both PFAS flow and their transformation.

2.3.1 Flow Mechanisms

In addition to partitioning, the transport mechanism (advection, dispersion, and diffusion) is important in the fate of PFAS. Advection can strongly influence the transport of PFAS, but it does not affect contaminant concentration (ITRC, 2018).

Dispersion disperses the contaminants in different directions due to changes in flow velocity. The concentration-gradient-driven flow, which can move the contaminant molecules into areas with a lower concentration, is referred to as molecular diffusion (ITRC, 2018). Although the diffusion in aquifer is hard to measure in some cases, it can contribute to the penetration process (Baduel et al., 2015).

2.3.2 Transformation Mechanisms

PFAS transformation includes biotic (living) and abiotic (nonliving) transformation, which can lead to other harmful chemicals. Hatton et al. (2018) showed that due to transformation, PFAS compounds found in the groundwater are considerably different from those in AFFF. Perfluoroalkyl acids (PFAAs) such as PFOA and PFOS can form from both biotic and abiotic transformation of polyfluorinated precursors. PFAAs are very stable, difficult to degrade, and mobile in the subsurface. This fact along with PFAAs' low sorption results in their accumulation in aquafers (Hatton et al., 2018). Because emerging PFAS have properties different from other contaminants, there is limited data regarding their transformation and, in general, their fate and transport.

2.4 Fate and Transport of PFAS

As discussed in the Introduction section of this chapter, the mechanism of partitioning, transport, and transformation within soils and aquafers has a significant role in determining and understanding the PFAS' fate and transport. Hydrophobic and lipophobic effects (Anderson et al., 2016; Xiao et al., 2017), electrostatic interactions (Zhao et al., 2014), and interfacial behaviors (Brusseau, 2018) are partitioning mechanisms that affect PFAS. Du et al. (2014) have shown that electrostatic and hydrophobic interactions are likely to control the sorption behavior of PFAS more than

other interactions. Some PFAS are more mobile, and they exist in the soluble phase due

to their low K_d (sorption partitioning coefficient), determined by:

$$K_d = C_S/C_W,$$ (2.1)

where C_s and C_w are the PFAS concentrations in sediment and water, respectively.

However, some PFAS with high K_d are more likely to be sorbed by soil and become

immobile. Li et al. (2018) reviewed studies to assess the effects of soil properties on the

sorption behavior of PFAS. Their review focused on the effects of clay content (due to

interfacial interaction), pH, and organic carbon (OC) due to hydrophobic partitioning on

the sorption behavior of PFAS. The main soil properties that control the sorption

behavior of PFAS and mitigate their transport within source zones, based on Li et al.

(2018), are as follows.

1. Organic carbon (OC): There are studies (Ahrens and Bundschuh, 2014; Chen

et al., 2013; You et al., 2010) indicating the existence of a strong relationship between the

sorption of PFAS and OC. These studies used the Freundlich equation (Equation 2.2) to

formulate sorption isotherms.

$$C_S = K_F C_W^n,$$ (2.2)

where K_F is the Freundlich sorption coefficient, and n provides an indication of the

nonlinearity. K_d is calculated using the following formula.

$$K_d = K_F C_W^{(n-1)}$$ (2.3)

The relation between the sorption of PFAS and OC has been expressed via figures

relating to K_d and the sediment OC content fraction (F_{OC}). Based on Figure 2.2, studies

(e.g., Milinovic et al., 2015; Chen et al., 2012) claimed that organic carbon can control

the sorption of PFAS. However, the study results of Barzen-Hanson et al. (2017)

demonstrated that the sorption process is more complex than what can only be calculated

using soil characteristics. This was consistent with most other findings in the

literature. However, Wang et al. (2020) assessed the partitioning behavior of PFAS and

claimed that OC does not have a significant effect on the partitioning behavior of

PFAS. Therefore, the OC content cannot be considered as the only factor that affects the

sorption behavior of PFAS.
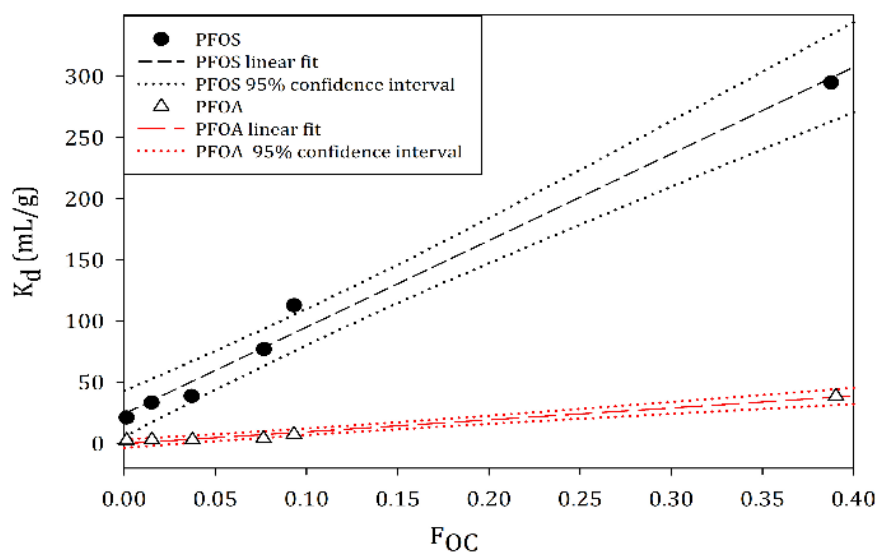
Fig. 2.2. Relation between the fraction of OC content and sorption of PFOA and PFOS (adapted from a figure by Milinovic et al., 2015).

2. pH: Like OC, there are different research results regarding the impact of pH on

the sorption of PFAS. Despite the fact that no direct exclusive physical relation between

pH and sorption has been developed, researchers often attempted to relate the two using

empirical linear models. Deng et al. (2012), Wang et al. (2012), and Yu et al. (2008)

observed that, like other anionic contaminants, the sorption of anionic PFAS decreased as

a result of increasing pH. On the other hand, You et al. (2010) and Zhou et al. (2013)

showed that the sorption of PFAS in the presence of Ca^{2+} or Mg^{2+} increased with

increasing pH while Milinovic et al. (2015) and Kwadijk et al. (2013) indicated that there

is not a demonstrable relation between pH and sorption of PFAS.

      3. Index cations and ionic strength: Cations can control the fate of anionic

PFAS in soil. Chen et al. (2012) assessed the effect of cations such as K^+, Ca^{2+}, Na^+, and

Mg^{2+}. They observed an increase in sorption due to the increase in the concentration of

Ca^{2+} and Mg^{2+} but found K^+ has no significant impact on sorption (Figure 2.3). Through

another review of previous research, Li et al. (2018) concluded that there is no significant

relation between the sorption of PFOA and PFOS with Ca^{2+} and/or with Na^+. In addition,

changes in the ionic strength led to a change in pH, and it is hard to determine which

parameter has a role in sorption (Higgins and Luthy, 2006).
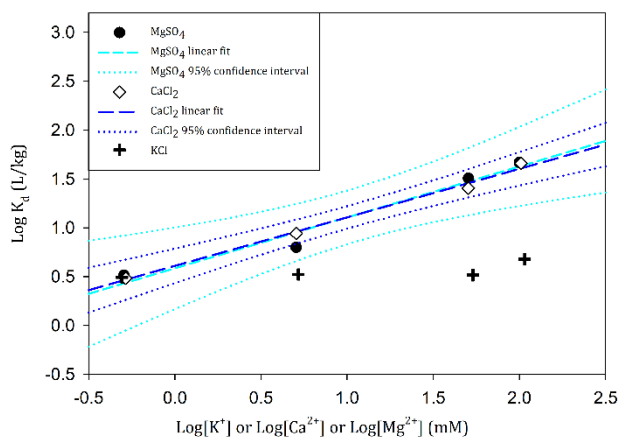
Fig. 2.3. Effects of monovalent and divalent metal cations' concentration on sorption coefficient (K_d) of PFOS (adapted from a figure by Chen et al., 2012).

      4. Clay content, cation exchange capacity (CEC), and anion exchange

capacity (AEC): there are very few studies that evaluated the role of clay content, but

they mostly demonstrate a strong relation between clay content and sorption of some

PFAS (Li et al., 2018). CEC and AEC are the capacity of soil to hold cations and anions,

respectively. Mejia-Avendaño et al. (2020) observed that the increase in the CEC value leads to an increase in cationic PFAS sorption. This can be justified based on the fact that high CEC can be translated to the availability of more cationic space (i.e., hole) within clays' microstructure (i.e., fundamental mineral unit blocks), which means more space for PFAS sorption. In contrast, the anion exchange capacity (AEC) can affect anionic compounds (Li et al., 2018). However, there is still not enough information regarding the impact of CEC and AEC.

Hence, the sorption behavior of PFAS is a compounded mechanism and cannot be explained only using one factor. There is usually a correlation between soil characteristics, e.g., it is probable to find higher contents of OC in clay-textured soils (Li et al., 2018). Therefore, to better understand the sorption behavior of PFAS, it is necessary to focus on several soil characteristics simultaneously.

2.5 Conclusions

The review in this paper resulted in the conclusion that phase-partitioning behaviors, such as sorption to soils and sediments, and transformation, control the fate, transport, and behavior of PFAS within the soil environment. Major soil/sediment components and properties that control sorption behavior include organic carbon (OC), pH, index cations and their ionic strength, clay content, and cation or anion exchange capacity (CEC or AEC). The sorption behavior of PFAS is complex and can be explained by only a combination of OC, pH, and clay content. Despite existing studies, there are still numerous unknowns, and specifically, there is a need for more research to understand the role of co-contaminants on the sorption behavior of PFAS and the role of

surface charge on the sorption of PFAS. In addition, more research is needed on a wider

range of PFAS chain compounds.

2.6 References

Ahrens, L., and Bundschuh, M. (2014): Fate and effects of poly-and perfluoroalkyl
substances in the aquatic environment: A review. *Environmental toxicology and chemistry*, *33*(9), 1921-1929.

Anderson, R. H., Long, G. C., Porter, R. C., & Anderson, J. K. (2016): Occurrence of
select perfluoroalkyl substances at US Air Force aqueous film-forming foam
release sites other than fire-training areas: Field-validation of critical fate and
transport properties. *Chemosphere*, *150*, 678-685.

Baduel, C., Paxman, C. J., & Mueller, J. F. (2015): Perfluoroalkyl substances in a
firefighting training ground (FTG), distribution and potential future release.
Journal of hazardous materials, *296*, 46-53.

Barzen-Hanson, K. A., Davis, S. E., Kleber, M., and Field, J. A. (2017): Sorption of
fluorotelomer sulfonates, fluorotelomer sulfonamido betaines, and a fluorotelomer
sulfonamido amine in national foam aqueous film-forming foam to the soil.
Environmental science & technology, *51*(21), 12394-12404.

Brusseau, M. L. (2018): Assessing the potential contributions of additional retention
processes to PFAS retardation in the subsurface. *Science of the Total Environment*, *613*, 176-185.

Buck, R. C., Franklin, J., Berger, U., Conder, J. M., Cousins, I. T., De Voogt, P., ... and
van Leeuwen, S. P. (2011): Perfluoroalkyl and polyfluoroalkyl substances in the
environment: terminology, classification, and origins. *Integrated environmental
assessment and management*, *7*(4), 513-541.

Chen, H., Zhang, C., Yu, Y., and Han, J. (2012): Sorption of perfluorooctane sulfonate
(PFOS) on marine sediments. Marine pollution bulletin, 64(5), 902-906.

Chen, Y. C., Lo, S. L., Li, N. H., Lee, Y. C., and Kuo, J. (2013): Sorption of perfluoroalkyl substances (PFASs) onto wetland soils. Desalination and Water Treatment, 51(40-42), 7469-7475.

Dauchy, X., Boiteux, V., Colin, A., Hémard, J., Bach, C., Rosin, C., and Munoz, J. F. (2019): Deep seepage of per-and polyfluoroalkyl substances through the soil of a firefighter training site and subsequent groundwater contamination. Chemosphere, 214, 729-737.

Deng, S., Zhang, Q., Nie, Y., Wei, H., Wang, B., Huang, J., ... and Xing, B. (2012): Sorption mechanisms of perfluorinated compounds on carbon nanotubes. Environmental Pollution, 168, 138-144.

Du, Z., Deng, S., Bei, Y., Huang, Q., Wang, B., Huang, J., and Yu, G. (2014): Adsorption behavior and mechanism of perfluorinated compounds on various adsorbents—A review. Journal of hazardous materials, 274, 443-454.

Hatton, J., Holton, C., and DiGuiseppi, B. (2018): Occurrence and behavior of per-and polyfluoroalkyl substances from aqueous film-forming foam in groundwater systems. Remediation Journal, 28(2), 89-99.

Higgins, C. P., and Luthy, R. G. (2006): Sorption of perfluorinated surfactants on sediments. Environmental science & technology, 40(23), 7251-7256.

Houde, M., De Silva, A. O., Muir, D. C., and Letcher, R. J. (2011): Monitoring of perfluorinated compounds in aquatic biota: an updated review: PFCs in aquatic biota. Environmental science & technology, 45(19), 7962-7973.

Houtz, E. F., Sutton, R., Park, J. S., and Sedlak, M. (2016): Poly-and perfluoroalkyl substances in wastewater: Significance of unknown precursors, manufacturing shifts, and likely AFFF impacts. Water Research, 95, 142-149.

ITRC (Interstate Technology & Regulatory Council). 2018: PFAS Fact Sheets PFAS-1. Washington, D.C.: Interstate Technology & Regulatory Council, PFAS Team. www.itrcweb.org.

Kwadijk, C. J. A. F., Velzeboer, I., and Koelmans, A. A. (2013): Sorption of perfluorooctane sulfonate to carbon nanotubes in aquatic sediments. Chemosphere, 90(5), 1631-1636.

Li, Y., Oliver, D. P., & Kookana, R. S. (2018): A critical analysis of published data to discern the role of soil and sediment properties in determining sorption of per and polyfluoroalkyl substances (PFASs). *Science of the Total Environment*, *628*, 110-120.

Martin, J. W., Mabury, S. A., Solomon, K. R., and Muir, D. C. (2003): Bioconcentration and tissue distribution of perfluorinated acids in rainbow trout (Oncorhynchus mykiss). Environmental Toxicology and Chemistry: An International Journal, 22(1), 196-204.

Mejia-Avendaño, S., Zhi, Y., Yan, B., and Liu, J. (2020): Sorption of polyfluoroalkyl surfactants on surface soils: Effect of molecular structures, soil properties, and solution chemistry. Environmental Science & Technology, 54(3), 1513-1521.

Milinovic, J., Lacorte, S., Vidal, M., and Rigol, A. (2015): Sorption behavior of perfluoroalkyl substances in soils. Science of the Total Environment, 511, 63-71.

Miyake, Y., Yamashita, N., Rostkowski, P., So, M. K., Taniyasu, S., Lam, P. K., and Kannan, K. (2007): Determination of trace levels of total fluorine in water using combustion ion chromatography for fluorine: a mass balance approach to determine individual perfluorinated chemicals in water. Journal of Chromatography A, 1143(1-2), 98-104.

Munoz, G., Desrosiers, M., Duy, S. V., Labadie, P., Budzinski, H., Liu, J., and Sauvé, S. (2017): Environmental occurrence of perfluoroalkyl acids and novel fluorotelomer surfactants in the freshwater fish Catostomus commersonii and sediments following firefighting foam deployment at the Lac-Mégantic railway accident. Environmental science & technology, 51(3), 1231-1240.

Oliver, D. P., Pan, Y. F., Anderson, J. S., Lin, T. F., Kookana, R. S., Douglas, G. B., and Wendling, L. A. (2013): Sorption of pesticides by a mineral sand mining by-

product, neutralised used acid (NUA). Science of the total environment, 442, 255-262.

Wang, F., Liu, C., and Shih, K. (2012): Adsorption behavior of perfluorooctanesulfonate (PFOS) and perfluorooctanoate (PFOA) on boehmite. Chemosphere, 89(8), 1009-1014.

Wang, S., Ma, L., Chen, C., Li, Y., Wu, Y., Liu, Y., and Wang, X. (2020): Occurrence and partitioning behavior of per-and polyfluoroalkyl substances (PFASs) in water and sediment from the Jiulong Estuary-Xiamen Bay, China. Chemosphere, 238, 124578.

Xiao, F. (2017): Emerging poly-and perfluoroalkyl substances in the aquatic environment: a review of current literature. Water Research, 124, 482-495.

Xiao, X., Ulrich, B. A., Chen, B., and Higgins, C. P. (2017): Sorption of poly-and perfluoroalkyl substances (PFASs) relevant to aqueous film-forming foam (AFFF)-impacted groundwater by biochars and activated carbon. Environmental science & technology, 51(11), 6342-6351.

You, C., Jia, C., and Pan, G. (2010): Effect of salinity and sediment characteristics on the sorption and desorption of perfluorooctane sulfonate at sediment-water interface. Environmental Pollution, 158(5), 1343-1347.

Yu, Q., Deng, S., and Yu, G. (2008): Selective removal of perfluorooctane sulfonate from aqueous solution using chitosan-based molecularly imprinted polymer adsorbents. Water Research, 42(12), 3089-3097.

Zhou, Q., Pan, G., and Zhang, J. (2013): Effective sorption of perfluorooctane sulfonate (PFOS) on hexadecyltrimethylammonium bromide immobilized mesoporous SiO2 hollow sphere. Chemosphere, 90(9), 2461-2466.

CHAPTER THREE: Multiphysics Numerical Modeling of Transient Transport of PFAS

ABSTRACT

The need to understand the fate and transport of per- and polyfluoroalkyl substances (PFAS) has grown due to the widespread contamination of the environment by them. PFAS are persistent, mobile, toxic manmade chemicals of great concern that contribute to the contamination of soil and groundwater. The presence of PFAS in unsaturated soil complicates their transport due to the impact of the air-water interface and solid-phase adsorption. The air-water interface can significantly increase the retention of PFAS during its transport. In this paper, a numerical model has been developed to study the transport of PFAS by coupling transient seepage and advection-dispersion, also accounting for the air-water interface and solid-phase adsorption. The numerical model was then used to study various scenarios.

3.1 INTRODUCTION

Per- and polyfluoroalkyl substances (PFAS) are synthetically fluorinated organic compounds of great concern due to the widespread contamination of the environment they cause. More than 4,000 PFAS compounds have been manufactured since the 1940s (Barzen-Hanson et al., 2017, Wang et al., 2017). This is due to PFAS's unique properties useful in industrial and commercial products such as fire resistance, dust suppression, oil repellence (lipophobic and hydrophobic properties), and remarkably high stability due to strong carbon-fluoride (C-F) bond (Buck et al., 2011). PFAS are known to be durable in the natural environment. The most common sources of PFAS in the environment are industrial facilities, landfills (leachate), wastewater treatment plants, consumer products (textile, cookware, etc.), and aqueous film-forming foams (AFFFs) (ITRC, 2018). AFFFs

are fire-fighting foams containing PFAS used for fire suppression at airports, fire training facilities, and chemical refineries. PFAS are known to be mobile, persistent, and very toxic chemicals that spread widely in the environment (Rayne and Forest, 2009; Ahrens, 2011; Krafft and Riess, 2015) and can lead to soil and groundwater contamination; thus, causing health hazards via drinking water contamination. The most common forms of PFAS found in the environment are perfluorooctane sulfonic acid (PFOS) and perfluorooctanoic acid (PFOA) (Lyu et al., 2018).

Better understanding of the fate and transport of PFAS in the subsurface is crucial for risk assessment as well as remediation of PFAS. Therefore, the objective of this research is to create a one-dimensional (1D) model coupling seepage and PFAS transport through the vadose zone and into groundwater by taking into consideration the advection, diffusion, and adsorption to the solid phase and air-water interfaces through different scenarios.

3.2 MATERIALS AND METHODS

3.2.1 Simulated Materials

Given this work is a numerical model with no experimental validation yet, the parameters used in the simulations of PFAS transport were obtained from a study conducted by Guo et al. (2020) on Accusand soil. However, the model is set up in a way that various types of soils and scenarios can be studied using this model. Guo et al. (2020) discuss how each parameter was obtained from various researchers (Brusseau et al., 2007; Araujo et al., 2015; Schaefer et al., 2019; Xu and Eckstein, 1995). Table 3.1 shows some of the parameters used. The listed parameters come from existing literature. In addition,

soils with different properties such as hydraulic conductivities and degrees of saturation were studied.

Table 3.1. Parameters used in the simulation

Parameters	Value	Unit
Bulk density, ρ_b	1.65	g/cm^3
Diffusion coefficient, D_0	5.4×10^{-6}	cm^2/s
Fitting parameter, K_f	0.055	-
Fitting parameter, N	0.85	-
Aqueous Concentration, C	12	Mg/L
Surface tension, σ	71	Dyn/cm
Gas constant, R	8.314	J/^{o}K/mol
Temperature, T	293.15	^{o}K

3.2.2 Methods

In this study, two numerical models, seepage and contaminant transport, were created and later coupled to study the fate and transport of PFAS using the MATLAB platform. The models solve the transient second order governing partial differential equations (PDEs) for seepage and PFAS transport using the finite-difference method (FDM). The simulated column (a 5cm-long soil domain) was discretized into a one-dimensional grid to solve for hydraulic head for seepage and aqueous concentration for transport of PFAS. The forward difference (Equation 3.1) was used to simulate the first derivative with respect to space and time, and the central difference (Equation 3.2) was used for the second derivative with respect to space.

$$\frac{\partial f}{\partial x} = \frac{f(x_{i+1}) - f(x_i))}{dx} \quad \text{(Forward Difference)} \tag{3.1}$$

$$\frac{\partial^2 f}{\partial x^2} = \frac{\partial}{\partial x}\left(\frac{\partial f}{\partial x}\right) = \frac{\partial}{\partial x}(f_x') = \frac{f(x_{i+1}) - 2f(x_i) + f(x_{i-1})}{dx^2} \quad \text{(Central Difference)} \tag{3.2}$$
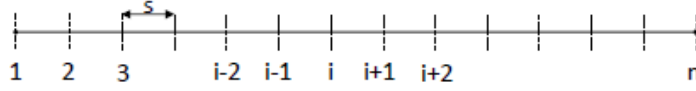
Figure 3.1. The schematic of the discretized domain.

3.2.2.1 Seepage Model

The transient seepage flow of water within the soil can be defined with the following 1D Equation by (Fredlund, 1997).

$$\vec{\nabla} \cdot v = -\frac{\partial \theta}{\partial t}, \tag{3.3}$$

where v is the seepage velocity, and θ is the volumetric water content equal to $n.S_w$, where n is the soil porosity, and S_w is the degree of water saturation.

Darcy's law ($v = -k_z.i$) can be applied to Equation (3.3). The right-hand side of Equation (3.3), i.e., the time variation in the volumetric content for a non-consolidating soil can be computed based on the specific/elastic capacity (i.e., retention) of water, m_v, and temporal variations of the hydraulic head, h. Hence:

$$\frac{\partial}{\partial z}\left(-k_z \frac{\partial h}{\partial z}\right) = -m_v \frac{\partial h}{\partial t}, \tag{3.4}$$

where k_z is the hydraulic conductivity, and $i = dh/dz$ is the hydraulic gradient. The specific or elastic capacity, m_v, is assumed ≈ 0.001 m^{-1} within unsaturated soils and ≈ 0.00001 m^{-1} within saturated soils.

To linearize the partial differential equation (3.4), the finite-difference method is applied to the discretized 1D grid for the transient seepage equation at each Node i can, hence, be simplified to the following form using the implicit approach (i.e., assuming h on the right-hand side of Equation (3.4) at time t^{k+1}, which is unknown).

$$h_{i-1}^{t^{k+1}}\left(\frac{k_i}{dz^2}\right) + h_i^{t^{k+1}}\left(\frac{-k_{i+1}}{dz^2} - \frac{k_i}{dz^2} - \frac{m_v}{dt}\right) + h_{i+1}^{t^{k+1}}\left(\frac{k_{i+1}}{dz^2}\right) = -\frac{m_v h_i^{t^{k+1}}}{dt},$$

(3.5)

where k_{i-1}, k_i, and k_{i+1} are the hydraulic conductivities at Nodes i-1, i, and i+1, respectively, while h_{i-1}, h_i, and h_{i+1} represent the hydraulic head at Nodes i-1, i, and i+1, respectively, over each time step. From the discretized equation, the hydraulic head can be determined at any node at any time. The unsaturated hydraulic conductivity can be written as a nonlinear function of h, shown in Equation (3.6).

$$k_i = \frac{k_0}{1+a_1|h_i-z_i|^{a_2}} \quad \rightarrow \quad k_i = \frac{k_0}{1+a_1|\frac{h_i^{t^k}+h_i^{t^{k+1}}}{2}-z_i|^{a_2}}, \qquad (3.6)$$

where k_i= unsaturated hydraulic conductivity at Node i, k_0= Saturated hydraulic conductivity, a_1 = constant (assumed 1), a_2 = constant (assumed 3), h= hydraulic (i.e., total) head, and z = elevation.

The coefficients k found using Equation (3.6) are nonlinear functions of the hydraulic head h, which again makes Equation (3.5) nonlinear. To be able to remove the complexity added by this nonlinearity and solve the linear system of equations for all nodes, these coefficients k need to be found, in a separate function, based on h averaged between times t^k and t^{k+1}. Since h at time t^{k+1} is unknown, a modified Crank-Nicolson successive iteration (Jordan Jr., 1981) scheme is used to converge to the best values of h at

time t^{k+1} and hydraulic conductivity k using Equation (3.6) based on the average of h between times t^k and t^{k+1}.

<u>Transport of PFAS</u>

Various transport processes contribute to the fate of PFAS upon the surface deposition and subsequent infiltration of PFAS into the vadose zone (Sharifan et al., 2021). The vadose zone can be considered a long-term source of PFAS continuation of groundwater (Shin et al., 2011, Brusseau, 2020) due to duration of time PFAS can spend in this zone. PFAS will almost always interact with soil before impacting groundwater. Various factors can affect the transport of PFAS both in water and soil, more specifically in the vadose zone where air and water coexist and can create fluid-fluid interfaces, e.g., air-water interface. PFAS are known to demonstrate surfactant-like properties, which makes their sorption to any fluid-fluid interface easier. PFAS accumulates at the air-water interface due to the hydrophobic and hydrophilic nature of PFAS at its tail and head, respectively, as shown by Figure 3.2. Thus, the unsaturated condition within the vadose zone provides a significant air-water interfacial area, A_{aw}, which can impact the overall PFAS migration (Sharifan et al., 2021).
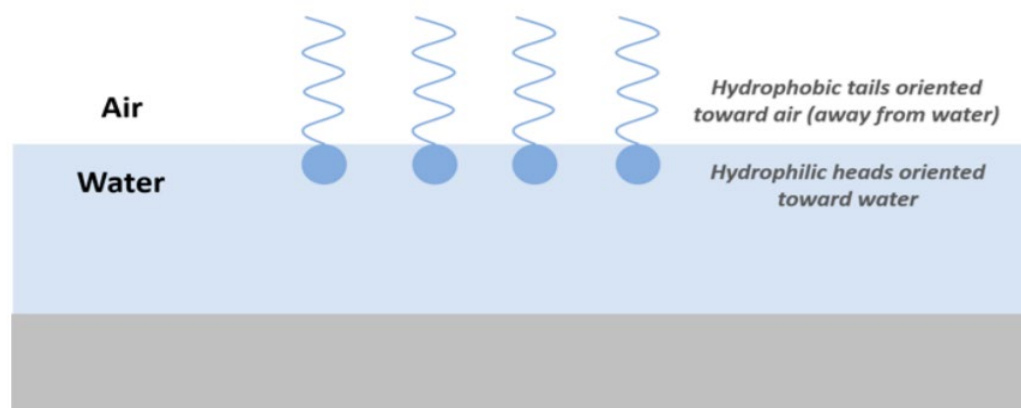
Figure 3.2. Example of expected orientation and accumulation of PFAS at air-water interface (D. Adamson, GSI)

Advection and diffusion are major mechanisms of PFAS flow that need to be considered when simulating the transport of PFAS. Advection consists of the bulk movement of solutes carried by flowing solvent (in here water), and diffusion is the spreading of the contaminant plume from a high concentration zone to a low concentrated zone (Freeze and Cherry, 1979). Both factors combined form an advection-diffusion equation shown by Equation (3.10).

$$\frac{\partial C}{\partial t} = -v_s \frac{\partial C}{\partial x} + D^* \frac{\partial^2 C}{\partial x^2}, \tag{3.7}$$

where D^*, the effective diffusion coefficient (cm^2/s), is given by Fick's Second Law and combines the longitudinal mechanical dispersion, D_L, with molecular diffusion, D_0; v_s is the seepage velocity (cm/s); and C is the aqueous concentration of the contaminant ($\mu mol/cm^3$).

The concentration of the adsorbed PFAS onto the air-water interface, C_{aw}, can be described using Equation (3.7) (Guo et al., 2020; Brusseau, 2007; Kim et al., 1997; Anwar, 2001).

$$C_{aw} = A_{aw}K_{aw}C, \tag{3.8}$$

where:

$$K_{aw} = \frac{-1}{RTC}\frac{\partial \sigma}{\sigma \ln C}, \tag{3.9}$$

where A_{aw} is the air-water interfacial area (cm^2/cm^3); K_{aw} is the air-water interfacial adsorption coefficient (cm^3/cm^2); R is the gas constant ($J/^\circ K/mol$); σ is the interfacial tension (dynes/cm); T is the temperature ($^\circ K$); C the aqueous concentration of PFAS ($\mu mol/cm^2$). On the other hand, the adsorption of PFAS onto the solid-phase, C_s, can be described using a Freundlich isotherm shown in Equation (3.8) (Brusseau, 2019a; Higgins & Luthy, 2006; Wei et al., 2017)

$$C_s = K_f C^N, \tag{3.10}$$

where K_f and N are fitting parameters found based on experimental data.

Therefore, the transport of PFAS is governed by the combined processes of seepage, advection, dispersion, and adsorption to the fluid-fluid and solid-fluid interfaces. Researchers have described it using an advection-dispersion equation with adsorption terms (Guo et al., 2020; Brusseau, 2019b; Kim et al., 1997).

$$\frac{\partial(\theta C)}{\partial t} + \rho_b \frac{\partial}{\partial t}k_f C^N + \frac{\partial}{\partial t}(A_{aw}k_{a\omega}C) + \frac{\partial}{\partial z}(\theta vC) - \frac{\partial}{\partial z}\left(\theta D \frac{\partial C}{\partial z}\right) = 0, \tag{3.11}$$

where ρ_b is the bulk density of the porous medium (g/cm^3); $V = q/\theta$ is the interstitial pore-water velocity (cm/s); q is the Darcy flux; and D is the dispersion/diffusion Coefficient (cm^2/s).

Using the forward and central difference methods ($\frac{\partial C_i}{\partial t} = \frac{C_i^{t^{k+1}}-C_i^{t^k}}{dt}$; $\frac{\partial^2 C_i}{\partial z^2} = \frac{C_{i+1}-2C_i+C_{i-1}}{dz^2}$; $\frac{\partial C_i}{\partial z} = \frac{c_{i+1}-c_{i-1}}{2\,dz}$; $\frac{\partial}{\partial t}C_i^N = NC_i^{N-1}\frac{\partial C_i}{\partial t}$), the PDE of Transport, i.e., Equation (3.11), can be discretized and linearized as follows.

$$C_{i+1}^{t^{k+1}}\left(-\frac{\theta_i^{t^{k+1}}v_i^{t^{k+1}}}{dz}+\frac{D_i^{t^{k+1}}\theta_{i+1}^{t^{k+1}}}{dz^2}+\frac{\theta_i^{t^{k+1}}D_{i+1}^{t^{k+1}}}{dz^2}\right)+C_i^{t^{k+1}}\left(3\frac{\theta_i^{t^{k+1}}v_i^{t^{k+1}}}{dz}-\right.$$

$$\frac{\theta_i^{t^{k+1}}v_{i+1}^{t^{k+1}}}{dz}-\frac{v_i^{t^{k+1}}\theta_{i+1}^{t^{k+1}}}{dz}-\frac{D_i^{t^{k+1}}\theta_{i+1}^{t^{k+1}}}{dz^2}+\frac{D_{i+1}^{t^{k+1}}\theta_i^{t^{k+1}}}{dz^2}+\frac{D_i^{t^{k+1}}\theta_i^{t^{k+1}}}{dz^2}-\frac{\theta_i^{t^{k+1}}}{dt}-\frac{F_i^{t^{k+1}}}{2dt}-\frac{F_i^{t^k}}{2dt}-$$

$$\left.A_{aw}\frac{k_{a\omega_i}^{t^{k+1}}}{dt}\right)+C_{i-1}^{t^{k+1}}\left(\frac{D_i^{t^{k+1}}\theta_i^{t^{k+1}}}{dz^2}\right)=C_i^{t^k}(-\frac{\theta_i^{t^{k+1}}}{dt}-\frac{F_i^{t^{k+1}}}{2dt}-\frac{F_i^{t^k}}{2dt}-A_{aw}\frac{k_{a\omega_i}^{t^k}}{dt},$$

$$(3.12)$$

where:

$$F = k_f\rho_b N C^{N-1} \qquad\qquad (3.13)$$

Like the case of hydraulic conductivity in Equation (3.5), coefficients F and K_{aw} are nonlinear functions of C, making Equation (3.12) nonlinear again. Similarly, these coefficients are found in a separate function using Equations (3.9) and (3.13) based on C averaged over times t^k and t^{k+1}. Since C at time t^{k+1} is unknown, the same modified Crank-Nicolson Successive Iteration (Jordan Jr., 1981) scheme is used in the separate function to converge to the best values of C at time t^{k+1} and K_{aw} and F based on C averaged between times t^k and t^{k+1}.

The MATLAB interface was then used to numerically solve Equation (3.12) to simulate several scenarios. The results of simulating those scenarios are discussed for a 5-cm-thick soil domain, discretized into a spatial and temporal grid of dz and dt equal to 0.5 cm and 10 seconds respectively.

3.3 RESULTS AND DISCUSSION

The developed code is only one-way coupled, even though the code is capable of simulating a two-way coupling. In this case, the seepage model simulates the transient

groundwater flow before PFAS is introduced into the soil. As shown in Figure 3.3, the groundwater moves from areas of higher hydraulic head toward those of lower hydraulic head, which was qualitatively validated against and was consistent with results by Freeze and Cherry (1979) in the literature. Then in the next step, the transport of PFAS in the same domain is simulated using the above-mentioned parameters and equations and the output data of the seepage code for the volumetric water content and seepage flow velocity. Different initial scenarios were then simulated and analyzed to confirm that the model works properly. The advection part of the simulation is not considered here to simplify the evaluation of the results for testing purposes. The following scenarios were simulated, accounting for diffusion, and adsorption onto the air-water and solid-phase interfaces at various degrees of water saturation. As seen in Figure 3.4, the PFAS concentration moves from a highly concentrated zone to a less concentrated zone, due to diffusion and adsorption terms. The change in the degree of water saturation retards the PFAS transport as expected. As shown in Figure 3.4, higher degrees of air-saturation (i.e., lower degrees of water-saturation) result in more retardation of PFAS transport through the vadose zone. The simulations for PFAS transport were conducted in increments of *15dt* over a period of 8000 seconds where dt = 10 sec. Therefore, Figure 3.4 shows vertical profiles of PFAS concentration are shown for every 15th curve in time.
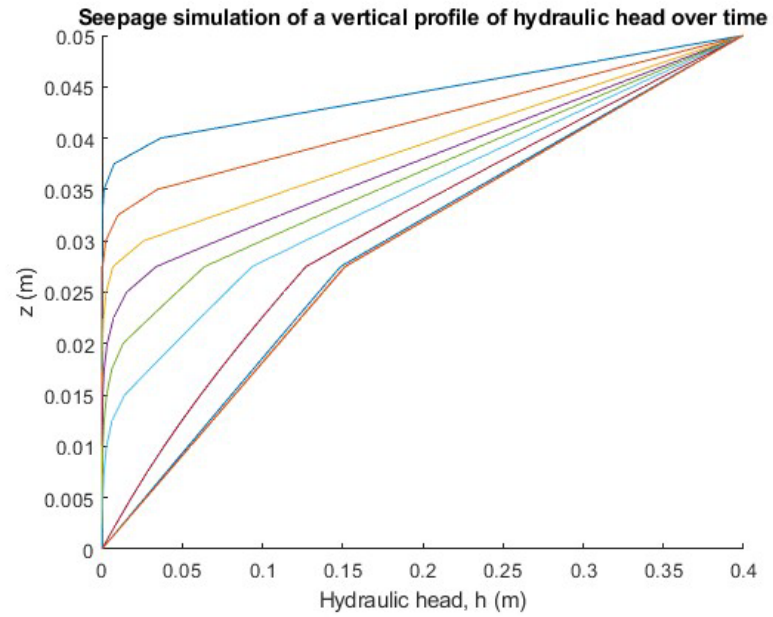
Figure 3.3. Seepage simulation: vertical profile of hydraulic head over time (every 10 seconds up to 8000 seconds) for unsaturated flow

(a) $S_w = 100\%$

28
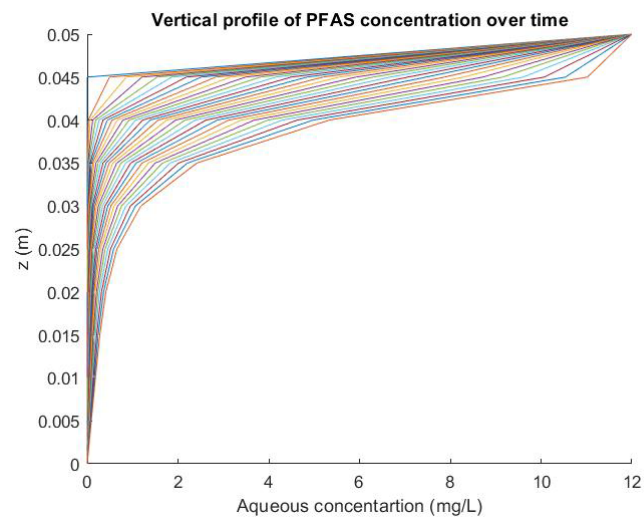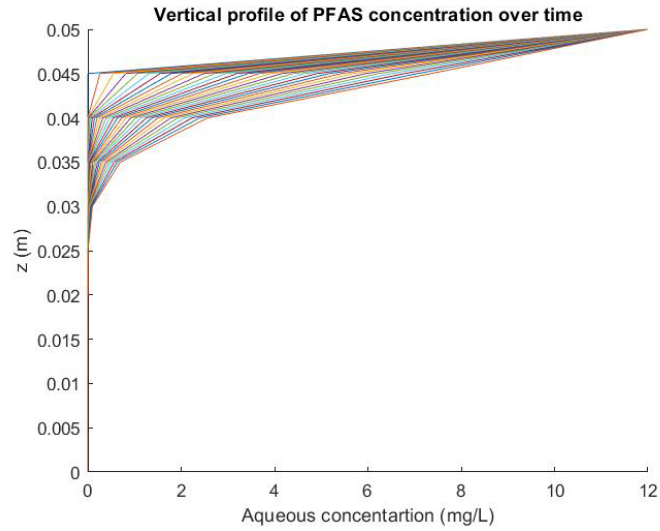
(b) $S_w = 73\%$
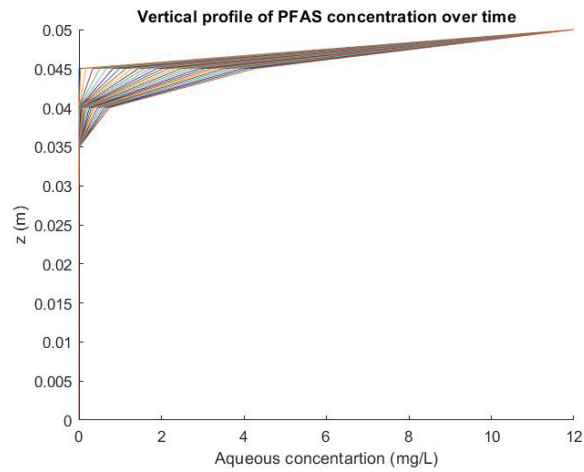
(c) $S_w = 47\%$

Figure 3.4. Progression of the vertical profile of PFAS' aqueous concentration over time (curves are 150 seconds (every 15th dt) apart up to 4500 seconds); Results are for the case of diffusion, dispersion, soil-phase adsorption, and micelles formed at air-water interface for various degrees of water saturation: (a) 100%, (b) 73%, and (c) 47%.

The retention of PFAS in the vadose zone is dependent on the soil matrix as well as the moisture content. Higher moisture contents result in lower retention due to the low availability of air-water interfacial areas (Silva et al., 2020; Lyu et al., 2018). Figure 3.5 shows how the concentration passing through a specific point (0.045 m below the top boundary) at a specific time (5 seconds after the PFAS is introduced into the sample) varies at the degree of saturation. As expected, at lower degrees of water-saturation, the transport of PFAS is retarded more (i.e., is slower), which demonstrates the increase in retardation due to low degrees of saturation (i.e., higher air content and air-water interface area).
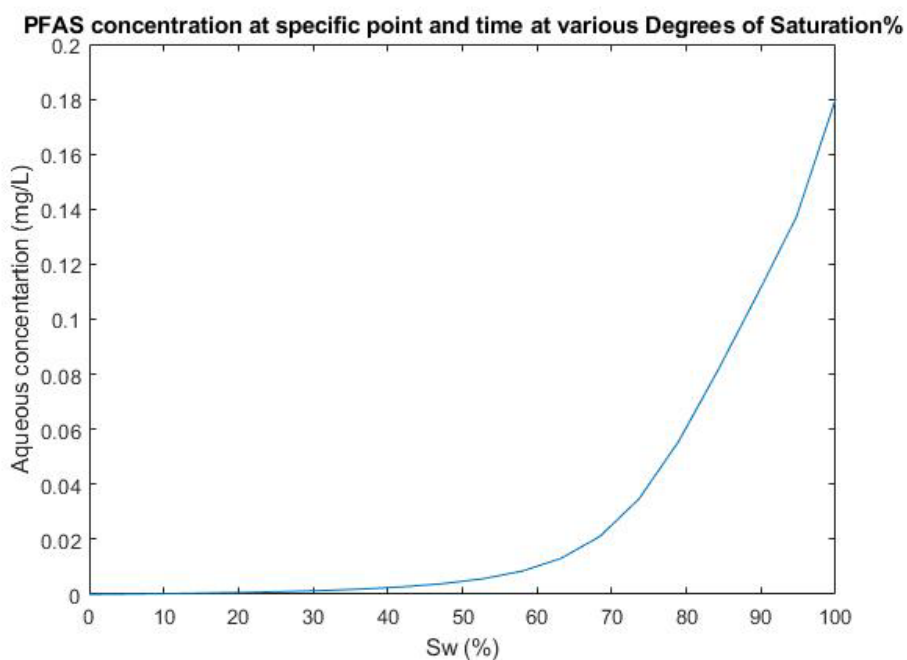
Figure 3.5. PFAS aqueous concentration at node 2 in space and node 5 in time (i.e., *z = 0.05 - dz* = cm and *t = 5dt = sec.*) at various degrees of water saturation

3.4 CONCLUSION

In this paper, a coupled one dimensional (1D) numerical model was introduced to simulate groundwater seepage flow and transport of PFAS. The model details were discussed, and a series of results for various scenarios was shown, which were consistent with the literature. However, the model is still being improved to account for more complex scenarios, and those improvements do not fit within the scope of this paper. Future steps can consist of testing the impact of advection and two-way coupling of seepage and PFAS transport where the effect of PFAS transport on the seepage by changing the properties of the flowing water (e.g., change in the hydraulic conductivity due to a change in the viscosity and density of water by the dissolved PFAS) can be simulated and analyzed.

3.5 REFERENCE

Ahrens, L., (2011). "Polyfluoroalkyl compounds in the aquatic environment: a review of their occurrence and fate." *J. Environ. Monit*, 13, 20−31.

Anwar, A. H. M. F., (2001). "Experimental determination of air−water interfacial area in unsaturated sand medium. New Approaches Characterizing Groundwater Flow." Proceedings of *the XXXI IAH Congress*, Munich, Germany, Sept 10−14, Vol. 2, pp 821−825.

Araujo, J.B., Mainhagu, J., and Brusseau, M. L. (2015). "Measuring air-water interfacial area for soils using the mass balance surfactant-tracer method." *Chemosphere*, 134, 199–202

Barzen-Hanson, K.A., Roberts, S.C., Choyke, S., Oetjen, K., McAlees, A., Riddell, N., McCrindle, R., Ferguson, P.L., Higgins, C.P., Field, J.A., (2017). "Discovery of 40 classes of per- and polyfluoroalkyl substances in historical aqueous film-forming foams (AFFF) and AFFF-impacted groundwater." *Environ. Sci. Technol*. 51,2047-2057.

Brusseau, M. L. (2019a). "Estimating the relative magnitudes of adsorption to solid-water and air/oil-water interfaces for per- and poly-fluoroalkyl substances." *Environmental Pollution*, *254*, 113102.

Brusseau, M. L. (2019b). "The influence of molecular structure on the adsorption of PFAS to fluid-fluid interfaces: Using QSPR to predict interfacial adsorption coefficients." *Water Research*, *152*, 148–158.

Brusseau, Mark L. (2020). "Simulating PFAS transport influenced by rate-limited multi-process retention." *Water Research*, Volume 168,115179.

Brusseau, M. L., Peng, S., Schnaar, G., and Murao, A. (2007). "Measuring air-water interfacial areas with X-ray microtomography and interfacial partitioning tracer tests." *Environmental Science & Technology*, 41(6), 1956–1961

Buck RC, Franklin J, Berger U, Conder JM, Cousins IT, De Voogt P, Jensen AA, Kannan K, Mabury, SA, and Van Leeuwen SP (2011). " Perfluoroalkyl and Polyfluoroalkyl Substances in the Environment: Terminology, Classification, and Origins." *Integrated environmental assessment and management*. 7:4:513. [PubMed: 21793199]

Freeze, A., and Cherry, J., (1979). "Groundwater." Prentice-Hall, Englewood Cliffs, New Jersey, 604 pages.

Fredlund, D. G., (1997). "Soil Mechanics for unsaturated soils." *China Architecture & Building Press*, Beijing Shi, China.

Guo, Bo & Zeng, Jicai and Brusseau, Mark. (2020). "A Mathematical Model for the Release, Transport, and Retention of Per- and Polyfluoroalkyl Substances (PFAS) in the Vadose Zone." *Water Resources Research*. 56. 10.1029/2019WR026667.

Higgins, C. P., and Luthy, R. G. (2006). "Sorption of perfluorinated surfactants on sediments." *Environmental Science & Technology*, 40(23),7251–7256.

Jordan Jr., Ernest David. (1981). "A modified Crank-Nicolson Method." *Master Thesis, Virginian Commonwealth University*. https://doi.org/10.25772/WAV4-6029

Krafft, M. P.; Riess, J. G. (2015). "Per- and polyfluorinated substances (PFAS): environmental challenges." Curr. Opin. Colloid Interface Sci. 20, 192−212

Kim, H., Rao, P. S. C., and Annable, M. D. (1997). "Determination of effective air-water interfacial area in partially saturated porous media using surfactant adsorption." *Water Resources Research*, *33*(12), 2705–2711.

Lyu Y., Brusseau M.L., Chen, W., Yan, N., Fu, X., and Lin, X. (2018). "Adsorption of PFOA at the Air-Water Interface during Transport in Unsaturated Porous Media." *Environ Sci Technol*. 2018 Jul 17 ;52(14) :7745-7753. DOI : 10.1021/acs.est.8b02348. E-pub, Jun 26. PMID: 29944343; PMCID: PMC6312111.

Rayne, S.; Forest, K. (2009). "Perfluoroalkyl sulfonic and carboxylic acids: A critical review of physicochemical properties, levels and patterns in waters and wastewaters, and treatment methods." *J. Environ. Sci. Health*, Part A: Toxic/Hazard. Subst. Environ. Eng., 44, 1145− 1199.

Schaefer, C., Drennan, D. M., Tran, D. N., Garcia, R., Christie, E., Higgins, C. P., and Field, J. A. (2019). "Measurement of aqueous diffusivities for perfluoroalkyl acids." *Journal of Environmental Engineering*, 145(11), 06019006.

Sharifan, H., Bagheri, M., Wang, D., Burken, J.G., Higgins, C. P., Liang, Y., Liu, J., Schaefer, C.E., and Blotevogel, J., (2021). "Fate and transport of per- and polyfluoroalkyl substances (PFASs) in the vadose zone." *Science of The Total Environment*, Volume 771, 145427.

Shin, H.M., Vieira, V.M., Ryan, P.B., Detwiler, R., Sanders, B., Steenland, K., and Bartell, S.M., (2011). "Environmental fate and transport modeling for perfluorooctanoic acid emitted from the Washington works facility in West Virginia." *Environ. Sci. Technol.,* 45 (4) (2011), pp. 1435-1442

Silva, J.A.K., McCray, J.E., Martin, W.A., (2020). "Final report: baseline data acquisition and numerical modeling to evaluate the fate and transport of PFAS within the vadose zone." SERDP project ER18-1389.

Wang, Zhanyun, DeWitt, Jamie C., Higgins, Christopher P., and Cousins, Ian T., (2017)." A never-ending story of per-and polyfluoroalkyl substances (PFAS)." *Environ. Sci. Technol*. 51,2508-6623.

Wei, C., Song, X., Wang, Q., and Hu, Z. (2017). "Sorption kinetics, isotherms, and mechanisms of PFOS on soils with different physicochemical properties." Ecotoxicology and Environmental Safety 142, 40–50.

Xu, M., & Eckstein, Y. (1995). "Use of weighted least-squares method in the evaluation of the relationship between dispersity and field scale." Groundwater, 33(6), 905–908.

CHAPTER FOUR: Effects of Adsorption Coefficients on PFAS Transport through

Vadose and Saturated Zones using a 1D Finite-difference Model

Abstract

Lately, a group of chemical compounds, Per-polyfluoroalkyl substances (PFAS), has been attracting attention due to their discovery in the environment as well as the risk they pose to human life, the environment, and groundwater. These compounds have been used in various products over the years and have, therefore, accumulated in the environment. PFAS exhibit various physiochemical properties, which make them useful in a variety of industries and products, adding to their pervasiveness. This coupled with their toxic effects on humans and biota leads to concerns regarding their fate and consequences to the ecosystem. The most investigated PFAS compounds are PFOA (Perfluorooctanoic acid) and PFOS (Perfluorooctane Sulfonic acid). To date, there are still many unanswered questions about the fate and transport of PFAS in unsaturated zones and how the underlying groundwater is affected. This is due to PFAS's ability to partition, bioaccumulate, and biotransform as well as due to their indestructibility due to the strong C-F bond.

In this paper, the fate and transport of PFAS (specifically PFOS) in both saturated and unsaturated zones are investigated through numerical modeling using the finite-difference method. This study investigates the effect of various transport processes (advection, diffusion, and adsorption) on the fate of PFAS in soil and groundwater. After the model was developed, the sensitivity of results to the selected spatial and temporal discretization (i.e., selection of time, dt, and space, dz) was analyzed. The results show very minimal (less than 2% of Change in stability sensitivity to dt within a range of 2 to 20 seconds (actually tested at 2, 5, 10, and 20 seconds) and to dz within a range of 0.001 to

0.02 m (actually tested at 0.001, 0.0025, 0.005, 0.0075, and 0.01 m). Multiple scenarios were then investigated using the model to understand the fate and transport of PFAS in both vadose and saturated zones to qualitatively verify the soundness of the results. The results need to be compared with undergoing experimental results as part of a separate research in order to validate the numerical model. This validation does not fit within the scope of this paper.

4.1 Introduction

Per- and polyfluoroalkyl substances, PFAS, are manmade chemicals that consist of a large class of more than 5,000 synthetically manufactured fluorinated organic compounds (Barzen-Hanson et al., 2017; Wang et al., 2017). PFAS has been used since the 1940s in various industrial and commercial products such as nonstick coatings, carpets and textiles, paper products, and in Aqueous Film-Forming Foam (AFFF) used for firefighting since the 1960s. PFAS is widely used in many products due to its unique properties, including water repellency as well as its fire resistance and chemical stability due to the strong Carbon and Fluorine (C-F) covalent bond. These properties have beneficial applications in industrial and consumer products. However, despite their industrial benefits, PFAS properties also make them persistent (indestructible) within the environment (Houtz et al., 2013; Buck et al., 2011). This persistence and PFAS's toxicity have led to environmental contamination mainly in drinking water, which has been linked to some human health issues such as fetal and placenta complications (Blake & Fenton, 2020; Nian et al., 2020), altering baby growth (Liew et al., 2018), and cancer (Viera et al., 2013), among many other health issues (Xu et al., 2020; Steenland et al., 2020). PFAS can contaminate the drinking water through various

sources such as deposition, leaching due to rainfall, landfill leachate, waste-water treatment facilities, and leaching due to the use of firefighting foams made of AFFF.

PFAS can also contaminate the drinking water through groundwater. Sharifan et al. (2021) demonstrated that PFAS interacted with soil and surface water before impacting the groundwater. The latter is why the vadose zone, i.e., the partially saturated area located above the water table, is known to be a significant source of PFAS release into the groundwater (Brusseau and Van Glubt, 2019; Barzen-Hanson et al., 2017). This suggests a great need to understand PFAS behavior in the vadose zone as studies show that PFAS largely accumulates in these areas. The vadose zone acts as a protective layer for groundwater through adsorption, partitioning, volatilization, and degradation processes that affect the transport and fate of contaminants (Sharifan et al., 2021). However, due to the small amount of desorption off the air-water interface and high level of PFAS toxicity, the vadose zone can become a hard-to-treat source of long-term PFAS release into the groundwater.

Limited research is available on the fate and transport of PFAS in the vadose zone due to PFAS behavior in the environment. PFAS is known to have surfactant properties that facilitate their sorption to fluid-fluid interfaces. The presence of air-water interfaces in the vadose zone contributes to the formation of PFAS micelles adsorbed to the air-water interfaces, retarding PFAS migration. Transport of both PFOA and PFOS in the unsaturated zone is complicated. While fluorinated compounds' persistence reduces the importance of degradation, the chemical properties of the compounds cause them to partition into a phase adsorbed onto the air-water interface. Partitioning to the air-water interface, according to recent research, may have significant implications for PFOS and

PFOA transport retardation (Brusseau, 2019a). Therefore, this study focuses on the development of a numerical model for the transport of PFAS in the vadose and saturated zones via coupling seepage and advection, hydrodynamic dispersion (i.e., molecular diffusion and mechanical dispersion), and adsorption to the solid phase and air-water interfaces. After the model was developed and before it could be used, an analysis on the sensitivity of the model results to the space and time discretization grids needs to be performed to narrow down the ranges of *dt* and *dz* at which, the model results are not sensitive to the selection of the time and space discretization grid size.

4.2 Background

To study the fate and transport of PFAS in the environment, the background of seepage, the transport process as well as PFAS's behavior and properties need to be first discussed.

4.2.1 Seepage

The seepage flow and its velocity are estimated based on a parameter referred to as hydraulic conductivity (i.e., soil permeability to water). Water diffuses through the soil from one point to another when there is a hydraulic head gradient. The relation between hydraulic head and velocity can be explained using Darcy's law.

$$Q = -K \frac{(h_B - h_A)}{L}, \tag{4.1}$$

where Q is the discharge (m^3/s), h is the total (hydraulic) head (m), L is the flow-path length (m), and k is the hydraulic conductivity of the soil (m/s).

The flow velocity can also be expressed as:

$$v = -k \frac{dh}{dl}, \tag{4.2}$$

where *dh/dl* is the hydraulic gradient, and *v* is the discharge (Darcy's) velocity (m/s). The negative sign shows that the water moves from areas with a higher total head toward areas with a lower total head, i.e., water flows in the direction of negative hydraulic gradient.

4.2.2 Transport Process

Various processes govern the fate and transport of PFAS through soil/sediment and groundwater. These transport processes include molecular diffusion, advection, mechanical dispersion, adsorption to the solid phase, adsorption to air-water interfaces, and chemical and biological transformation. Chemical and biological transformation does not ft within the scope of this paper. Molecular diffusion refers to the transport of PFAS from points of high concentration of those with lower concentration. If there is a background seepage flow (caused by diffusion of water from high hydraulic gradient to lower hydraulic gradient), the flowing water will carry PFAS using an advective flow. The advective flow of PFAS through porous media along a tortuous path causes longitudinal and transverse mechanical dispersion. Molecular diffusion and mechanical dispersion combined are referred to as hydrodynamic dispersion. In addition to the adsorption of PFAS onto soil solid phase, the adsorption of PFAS onto air-water interfaces also impact the transport of PFAS and more specifically to PFOA and PFOS (Lyu et al., 2018; Brusseau, 2019a) due to their molecular structure. Volatilization was not investigated in this study for PFAS because the volatility of both PFOA and PFOS is negligible (Ding & Peinenburg, 2013).

Molecular Diffusion, Advection, and Mechanical Dispersion

Molecular diffusion, advection, and mechanical dispersion are inherent to the transport of all solutes through porous media. To understand the effect of these processes,

a commonly used equation known as the one-dimensional (1D) Advection-Dispersion equation (ADE) is used in this study, which can be written in its simplest transient form as:

$$\frac{\partial(\theta C)}{\partial t} = -\frac{\partial}{\partial z}(\theta v C) + \frac{\partial}{\partial z}\left(\theta D^* \frac{\partial C}{\partial z}\right), \tag{4.3}$$

where θ is the volumetric water content, C is the aqueous concentration of PFAS, v is the discharge velocity, and D^* is the longitudinal component of the hydrodynamic dispersion coefficient that represents both the molecular diffusion and the advection-driven mechanical dispersion given by:

$$D^* = D + a_L . v, \tag{4.4}$$

where a_L is the dispersivity (cm), and D is the molecular diffusion coefficient (cm^2/s).

The ADE is only used to describe the transport of nonreactive and nonadsorptive solutes. In the presence of adsorption, the adsorption terms need to be reflected in Equation (4.3). Adsorption is the process of partitioning of PFAS from the aqueous form into the adsorbed phase onto other two phases, i.e., solid particles and air-water interface. Hence, the adsorption to the solid phase and the adsorption to all air-water interfaces are governed by their own mechanisms.

<u>Solid-Phase Adsorption</u>

The solid-phase-adsorption term describes the interactions or processes that bind a compound to the surface of the soil particles. According to Li et al. (2018), PFAS has shown possible adsorption to soil particles due to both electrostatic and hydrophobic interactions. These adsorption mechanisms can be defined using a series of equations quantifying their effects on the overall transport. The solid-phase adsorption can be described using partitioning coefficients such as K_d:

$$K_d = \frac{C_s}{C_{aq}}, \tag{4.5}$$

where K_d is the partitioning coefficient to the solid phase, C_s is the concentration of the compound adsorbed onto solids, and C_{aq} is the concentration in the solution, in this case, the aqueous concentration. Depending on the nature and regime governing the adsorption, various models are used. The regime governing the adsorption of PFAS onto the solid phase at equilibrium can be described using different isotherms such as the Freundlich isotherm equation as follows.

$$C_s = K_f C^N, \tag{4.6}$$

where K_f and N are fitting parameters found based on experimental data. Therefore, the adsorption onto the solid-phase term of Equation (4.7) should be incorporated into the transport equation (Equation 4.3).

$$[\frac{\partial(\theta C)}{\partial t}]_{due\ to\ soprtion} = \rho_b \frac{\partial}{\partial t} k_f C^N, \tag{4.7}$$

where C is the aqueous concentration of PFAS; ρ_b is the bulk density of the porous medium (g/cm^3); θ is the volumetric water content; K_f and N are fitting parameters found based on experimental data.

Air-water Interface Adsorption

Another process that significantly affects the fate and transport of PFAS within the unsaturated zones is the adsorption to air-water interfaces (AWIs), referred to as micelles formation. This is because PFAS acts as a surfactant due to its molecular structure containing a hydrophobic "tail" and hydrophilic "head."

As with partitioning to the solid phase, adsorption to AWIs can also be described using a partitioning coefficient, *Kaw*.

$$K_{aw} = \frac{C_{aw}}{C_{aq}}, \tag{4.8}$$

where K_{aw} is the AWI partitioning coefficient, C_{aw} is the concentration adsorbed onto the air-water interface, and C_{aq} is the concentration in the solution. K_{aw} can also be expressed as follows.

$$K_{aw} = \frac{-1}{RTC} \frac{\partial \sigma}{\sigma \ln C}, \tag{4.9}$$

where A_{aw} is the air-water interfacial area (cm^2/cm^3); K_{aw} is the air-water interfacial adsorption coefficient (cm^3/cm^2); R is the gas constant (in J/K/mol); σ is the interfacial tension (in dynes/cm); T is the temperature (°K); C is the aqueous concentration of PFAS (in µmol/cm^2).

Therefore, the adsorption at the air-water interface (Equation 4.10) should be incorporated into the transport equation (Equation 4.3) as follows.

$$\frac{\partial(\theta C)}{\partial t} = \frac{\partial}{\partial t}(A_{aw} k_{a\omega} C). \tag{4.10}$$

Therefore, the overall transport of PFAS can be described using the ADE supplemented with adsorption terms as follows (Guo et al., 2020; Brusseau, 2019b; Kim et al., 1997).

$$\rho_b \frac{\partial}{\partial t} k_f C^N + \frac{\partial}{\partial t}(A_{aw} k_{a\omega} C) + \frac{\partial}{\partial z}(\theta v C) - \frac{\partial}{\partial z}\left(\theta D \frac{\partial C}{\partial z}\right) = -\frac{\partial(\theta C)}{\partial t} \tag{4.11}$$

4.3 Materials and Methods

4.3.1 Materials

This study is designed to numerically simulate various scenarios of 1D PFAS transport through a lab-scale experimental column with a diameter of 4 cm and length of 5 cm. The initial hydraulic head, H_1, at the inlet (top of the column) is maintained constant at 42 cm and the outlet head H_2 (at the bottom) can be either maintained at a constant value of 0 cm or be allowed to increase. The PFAS investigated in this research is PFOS, with a constant concentration supply of 12 mg/L at the inlet at the top of the column. This model accounts for two types of soil with equal lengths, but different hydraulic conductivities

stacked up within the column. The parameters used in this study were obtained from various literature (Guo et al. 2020; Brusseau et al., 2007; Araujo et al., 2015; Schaefer et al., 2019; Xu and Eckstein, 1995).

4.3.2 Methodology

This study consists of two numerical models, seepage and contaminant transport, both developed using the MATLAB interface. The two models can be coupled to simulate and investigate the fate and transport of PFAS in the presence of background seepage within both saturated and unsaturated environments. The finite-difference method (FDM) was used to solve the governing partial differential equations (PDEs) for seepage and PFAS transport.

This study employs two types of boundary conditions: (i) Dirichlet and (ii) Neumann boundary conditions. The Dirichlet boundary condition is used to simulate constant hydraulic head and concentration for the seepage model and transport, respectively, while the transport model also employs Neumann boundary conditions. The Dirichlet boundary condition simulates a fixed value (e.g., fixed hydraulic head within the seepage model and fixed concentration within the transport model). The Neuman boundary condition keeps the derivatives of the hydraulic head and concentration constant within the seepage and transport model, respectively.

Seepage Model

Seepage is governed by the mass-continuity (conservation of mass) equation. The flow velocity is governed by Darcy's law as mentioned.

Using a differential form, the conservation of mass equation can be written as:

$$\frac{\partial \rho}{\partial t} + \vec{\nabla}.(\rho\vec{v}) = 0, \tag{4.12}$$

where ρ is the fluid density (m³/s), t is the time (s), and $\vec{v}$ is Darcy's (aka, discharge) flow velocity vector (m/s).

Assuming the fluid is incompressible and the change in the density due to the change in the PFAS concertation is negligible, the density of the fluid can be considered constant. Therefore, the mass-continuity equation (4.12) can be simplified to a volume-continuity equation written as follows.

$$\vec{\nabla}.\vec{v} = 0 \tag{4.13}$$

The velocity vector can be expressed in terms of hydraulic conductivity and hydraulic head using Darcy's law (Equation 4.14).

$$\vec{v} = -k_z i, \tag{4.14}$$

where k is the hydraulic head, and i is the hydraulic gradient also known as $\vec{\nabla}h$.

Equation (4.14) can also be written as:

$$\vec{v} = -k\vec{\nabla}h \tag{4.15}$$

For 1D, the hydraulic gradient i can be written as follows:

$$i = \vec{\nabla}h = \frac{\partial h}{\partial z}\overrightarrow{a_z}, \tag{4.16}$$

where $\overrightarrow{a_z}$ is the unit vector in the Z-direction.

The governing equation of transient seepage flow can then be written as (Fredlund, 1997):

$$\vec{\nabla}\cdot\vec{v} = -\frac{\partial\theta}{\partial t}, \tag{4.17}$$

where v is the seepage velocity, and θ is the volumetric water content $= n.S_w$, where n is the soil porosity, and S_w is the degree of water saturation. Assuming that the volumetric water content can be computed based on the specific/elastic capacity (i.e., retention) of water, m_v, and temporal variations of the hydraulic head, h, the governing equation can be written as:

$$\vec{\nabla}.\left(-kz\vec{\nabla}h\right) = \frac{\partial\theta}{\partial t} \tag{4.18}$$

In 1D, Equation (4.18) can be simplified as:

$$\frac{\partial}{\partial z}\left(-k_z \frac{\partial h}{\partial z}\right) = -m_V \frac{\partial h}{\partial t} \tag{4.19}$$

For the seepage model, the Dirichlet boundary condition was used to simulate the constant head where at Node 1, h is equal to H_1, and at Node m, the total head h is equal to H_2.

Within the finite-difference method, forward and central difference methods were applied to the first-degree partial derivatives with respect to space. The domain was discretized, and Equation (4.19) was linearized using the finite-difference method as follows.

$$h_{i-1}^{t^{k+1}}\left(\frac{k_i}{dz^2}\right) + h_i^{t^{k+1}}\left(\frac{-k_{i+1}}{dz^2} - \frac{k_i}{dz^2} - \frac{m_v}{dt}\right) + h_{i+1}^{t^{k+1}}\left(\frac{k_{i+1}}{dz^2}\right) = -\frac{m_v h_i^{t^k}}{dt}, \tag{4.20}$$

where superscripted terms t^k and t^{k+1} refer to before and after the time interval dt. Then, each hydraulic head on the left-hand side is written as the weighted average of the values at the two times t^{k+1} and t^k, (similar to the Crank-Nicolson method) to allow more stability at large dt. However, coefficients k_i and k_{i+1} (hydraulic conductivity at Nodes i and $i+1$) for the transient case are nonlinear functions of h, preventing Equation (4.20) from becoming linear, if expanded as a function of h. The method to allow treating this system of equations as a linear system within the discretized domain is described in the next section. As mentioned, Since h at time t^{k+1} is unknown, coefficients k_i and k_{i+1} (hydraulic conductivity at Nodes i and $i+1$) were found using based on the h averaged over times t^k and t^{k+1} using the Modified Iterated Crank-Nicolson Method (Jordan Jr., 1981). In other words, a successive iteration was pursued within each time step, dt, until k from Equation (4.22) and h converge.

<u>Successive Iteration to Find Hydraulic Conductivity within Each Time Step</u>:

For the saturated soil, the specific/elastic capacity, m_v, is assumed 0.00001, to simulate the incompressibility of water and hence saturated soil. However, in unsaturated soil, the hydraulic conductivity can be calculated using the following equation.

$$k_i^{t^k} = \frac{k_0}{1+a_1\left|h_i^{t^k}-z_i^{t^k}\right|^{a_2}}, \tag{4.21}$$

where k_0 is the saturated hydraulic conductivity; a_1 and $a2$ are constants assumed to be 1 and 3, respectively; $h_i^{t^k}$ is the hydraulic head at Node I and time t^k; and $z_i^{t^k}$ is the elevation head at Node i.

While h_i, in Equation (4.21) for hydraulic conductivity, can be $h_i^{t^k}$ or $h_i^{t^{k+1}}$ or the average. For this study, we used the average h over dt as in the Modified Iterated Crank-Nicolson Method (Jordan Jr., 1981) method, as a method to allow more stability for larger values of dt for the model. The hydraulic conductivity needs to be calculated within each time step and takes the form of Equation (4.22).

$$k_i^{t^k} = \frac{k_0}{1+a_1\left|\frac{h_i^{t^k}+h_i^{t^{k+1}}}{2}-z_i^{t^k}\right|^{a_2}} \tag{4.22}$$

This, however, makes the governing equation (4.20) nonlinear, preventing the creation of a linear system of equations for all nodes. Hence, to be able to solve the system of equations within the discretized domain as a linear system, coefficients k_i and k_{i+1} (hydraulic conductivity at Nodes i and $i+1$) were found based on the h averaged over times t^k and t^{k+1} using the Modified Iterated Crank-Nicolson Method (Jordan Jr., 1981). In other words, a successive iteration was pursued within each time step, dt, until each of k from Equation (4.22) and h converge. Basically, within each time step, since $h_i^{t^{k+1}}$ is unknown, the code initially uses the initial $h_i^{t^k}$ to find the hydraulic conductivity. Then, the solver is

run to find $h_i^{t^{k+1}}$, which will then be used to update the hydraulic conductivity (using

Equation 4.22) and consequently $h_i^{t^{k+1}}$. This updating process s successively iterated to

find $h_i^{t^{k+1}}$ based on $h_i^{t^k}$ and the ever-updating hydraulic conductivity. This is continued

until both the hydraulic conductivities and $h_i^{t^{k+1}}$ converge to the same answers. Once this

is accomplished, the code moves on to the next time step. From the calculations of the

hydraulic head, the seepage velocity and volumetric water content are then determined.

Transport of PFAS

As mentioned, the overall transport of PFAS is governed by the combination of

advection, hydrodynamic dispersion, and adsorption at solid (i.e., soil particles) and air-

water interfaces described using Equation 4.11 (Guo et al., 2020; Brusseau, 2019b; Kim et

al., 1997).

$$\rho_b \frac{\partial}{\partial t} k_f C^N + \frac{\partial}{\partial t}(A_{aw} k_{a\omega} C) + \frac{\partial}{\partial z}(\theta v C) - \frac{\partial}{\partial z}\left(\theta D \frac{\partial C}{\partial z}\right) = -\frac{\partial(\theta C)}{\partial t}, \qquad (4.11)$$

where ρ_b is the bulk density of the porous medium (g/cm³); $v = q/\theta$ is the interstitial pore-

water velocity (cm/s); q is the Darcy flux; and D is the dispersion/diffusion coefficient

(cm²/s).

As mentioned, the transport equation was simulated a Dirichlet boundary condition

was considered. The Dirichlet boundary conditions simulate the constant supply of PFAS

concentration at the inlet (the top) of the column and the outlet exposed to an abundance

of freshwater ($C = 0$), where no accumulation of PFAS occurs at the outlet (the bottom) of

the column. This can be expressed as.

At any given time, t, and Node 1, $C_1^t = C_0$, where C_1^t is the concentration at time t

and Node 1, and C_0 is the initial concentration.

At all times t and Node m, $C_m^t = 0$, where m is the last node, C_m^t is the concentration at time t and Node m.

Another boundary condition that was considered in this simulation is the Neumann boundary condition specifying the values of the derivative of concentration applied at the domain boundary to be zero. The Newmann boundary condition allows to simulate the transport of PFAS assuming there is an accumulation of PFAS concentration at the outlet (bottom) allowing a breakthrough of concentration. This can be expressed as follows.

At any given time, t, and Node 1, $C_1^t = C_0$, where C_1^t is the concentration at time t and Node 1, and C_0 is the initial concentration. In addition, at all times t at Node m, $\frac{\partial C_m}{\partial t} = 0 \rightarrow C_m^t = C_{m-1}^t$, where m is the last node, C_m^t is the concentration at time t and Node m, and C_{m-1}^t is the concentration at time t and Node m-1 (the node before the last).

Similar to the seepage model, a finite-difference numerical model was developed in MATLAB interface to analyze the transport of PFAS. Each transport mechanism was initially simulated and tested before, and they were combined. In this case, the effects of advection-diffusion only, solid-phase adsorption, and air-water-interface adsorption as well as various combinations of them were simulated.

Each partial derivative was linearized using FDM over the discretized domain. Below are the results of the application of the FDM to linearize transport equations.

Advection diffusion:

The change in concentration due to advection and diffusion together can be combined as follows.

$$\frac{\partial(\theta C)}{\partial t} = -\frac{\partial}{\partial z}(\theta v C) + \frac{\partial}{\partial z}\left(\theta D^* \frac{\partial C}{\partial z}\right) \qquad (4.23)$$

Equation (4.23) can be discretized using the finite-difference method as follows.

$$C_{i+1}^{t^{k+1}}\left(\frac{D_i\theta_{i+1}}{dz^2}+\frac{\theta_iD_{i+1}}{dz^2}-\frac{D_i\theta_i}{dz^2}-\frac{\theta_iv_i}{dz}\right)-C_i^{t^{k+1}}\left(\frac{D_i\theta_{i+1}}{dz^2}+\frac{\theta_iD_{i+1}}{dz^2}+\frac{\theta_i}{dt}+\frac{\theta_i^{t^{k+1}}-\theta_i^{t^k}}{2dt}+\frac{v_i\theta_{i+1}^{t^{k+1}}}{2dz}-\right.$$

$$\left.\frac{v_i\theta_i^{t^{k+1}}}{2dz}+\frac{\theta_iv_{i+1}^{t^{k+1}}}{2dz}-\frac{\theta_iv_i^{t^{k+1}}}{2dz}-\frac{\theta_iv_i}{dz}\right)+C_{i-1}^{t^{k+1}}\left(\frac{\theta_iD_i}{dz^2}\right)=-C_i^{t^k}\left(-\frac{\theta_i^{t^{k+1}}}{2dt}+\frac{\theta_i^{t^k}}{2dt}+\frac{\theta_i}{dt}-\frac{v_i\theta_{i+1}^{t^{k+1}}}{2dz}+\right.$$

$$\left.\frac{v_i\theta_i^{t^{k+1}}}{2dz}-\frac{\theta_iv_{i+1}^{t^{k+1}}}{2dz}+\frac{\theta_iv_i^{t^{k+1}}}{2dz}\right),\quad(4.24)$$

where a scheme similar to Crank-Nicolson (Jordan Jr., 1981) was used over each time step, i.e., $\theta_i=\frac{\theta_i^{t^{k+1}}+\theta_i^{t^k}}{2}$ and $D_i=\frac{D_i^{t^{k+1}}+D_i^{t^k}}{2}$ to find more accurate values of the volumetric content. The same modified iterated Crack-Nicolson method is applied to converge to best values for the diffusion coefficient for each time step.

Solid-phase adsorption term:

The change in concentration due to the solid-phase adsorption can be written as:

$$\frac{d(\theta C)}{dt}=-\rho_b k_f\frac{d}{dt}C^N,\qquad(4.25)$$

which can be discretized as follows.

$$-\frac{FC_i^{t^{k+1}}}{dt}+\frac{FC_i^{t^k}}{dt}=C_i^{t^{k+1}}\left(\frac{\theta_i}{dt}+\frac{\theta_i^{t^{k+1}}}{2dt}+\frac{\theta_i^{t^k}}{2dt}\right)+C_i^{t^k}\left(\frac{\theta_i^{t^{k+1}}}{2dt}-\frac{\theta_i^{t^k}}{2dt}-\frac{\theta_i}{dt}\right),\qquad(4.26)$$

where $F=-\rho_b k_f N C^{N-1}$.

Coefficient F is nonlinear functions of C, making Equation (4.26) nonlinear again. These coefficients are found in a separate function based on C averaged over times t^k and t^{k+1}.

Since C at time t^{k+1} is unknown, the same modified Crank-Nicolson Successive Iteration (Jordan Jr., 1981) scheme is used in the separate function to converge to the best values of C at time t^{k+1} and F based on C averaged between times t^k and t^{k+1}.

Air-water-interface adsorption:

The change in concentration due to the formation of micelles adsorbed onto all air-water interfaces can be written as:

$$\frac{\partial(\theta C)}{\partial t} = -\frac{\partial}{\partial t}(A_{aw}k_{a\omega}C), \tag{4.27}$$

which can be discretized as:

$$C_i^{t^{k+1}}\left(-k_{a\omega_i}\frac{A_{aw_i}^{t^{k+1}}}{2dt} + k_{a\omega_i}\frac{A_{aw_i}^{t^k}}{2dt} - A_{aw_i}\frac{k_{aw_i}^{t^{k+1}}}{2dt} + A_{aw_i}\frac{k_{aw_i}^{t^k}}{2dt} - \frac{A_{aw_i}k_{aw_i}}{dt}\right) +$$

$$C_i^{t^k}\left(-k_{a\omega_i}\frac{A_{aw_i}^{t^{k+1}}}{2dt} + k_{a\omega_i}\frac{A_{aw_i}^{t^k}}{2dt} - A_{aw_i}\frac{k_{aw_i}^{t^{k+1}}}{2dt} + A_{aw_i}\frac{k_{aw_i}^{t^k}}{2dt} + \frac{A_{aw_i}k_{aw_i}}{dt}\right) =$$

$$C_i^{t^{k+1}}\left(\frac{\theta_i}{dt} + \frac{\theta_i^{t^{k+1}}}{2dt} - \frac{\theta_i^{t^k}}{2dt}\right) + C_i^{t^k}\left(\frac{\theta_i^{t^{k+1}}}{2dt} - \frac{\theta_i^{t^k}}{2dt} - \frac{\theta_i}{dt}\right),$$

$$(4.28)$$

where the Modified Iterated Crank-Nicolson Method (Jordan Jr., 1981) was used to find a more accurate value for the volumetric-water content, i.e., $\theta_i = \frac{\theta_i^{t^{k+1}} + \theta_i^{t^k}}{2}$.

Coefficients F and k_{aw} are nonlinear functions of C, making Equation (4.28) nonlinear again. These coefficients are found in a separate function based on C averaged over times t^k and t^{k+1}. Since C at time t^{k+1} is unknown, the same modified Crank-Nicolson

Successive Iteration (Jordan Jr., 1981) scheme is used in the separate function to converge to the best values of C at time t^{k+1} and K_{aw} and F based on C averaged between times t^k and t^{k+1}.

Once the transport model was completed, it was coupled with the seepage model to study the overall transport of PFAS in the vadose or saturated zone when there is seepage flow.

4.4 Results and Discussion

4.4.1 Sensitivity Analysis

Before various scenarios are studied, the sensitivity of the results of the numerical model to the resolution of the time and space discretized grids (i.e., the size of dt and dz) needs to be analyzed. This will determine the ranges of dt and dz at which the model is independent of dt and dz selection. Figures 4.1 and 4.2 show very little sensitivity (less than 2% of sensitivity) to dz and dt over the shown range. Figure 4.2 shows a two-dimensional (2D) figure, which is a combination of Figures 4.1(a) and 4.1(b).

(a)   (b)
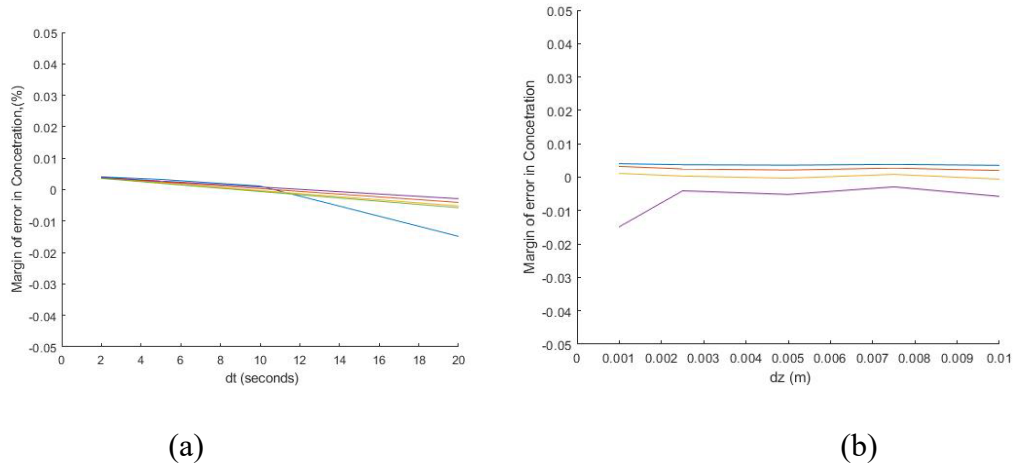
**Figure 4.1. Sensitivity analysis: (a) sensitivity to time-discretization grid size for *dt* =
2, 5, 10, 20 sec.; (b) sensitivity to space-discretization grid size for *dz* = 0.001, 0.0025,
0.005, 0.0075, 0.01 m.**
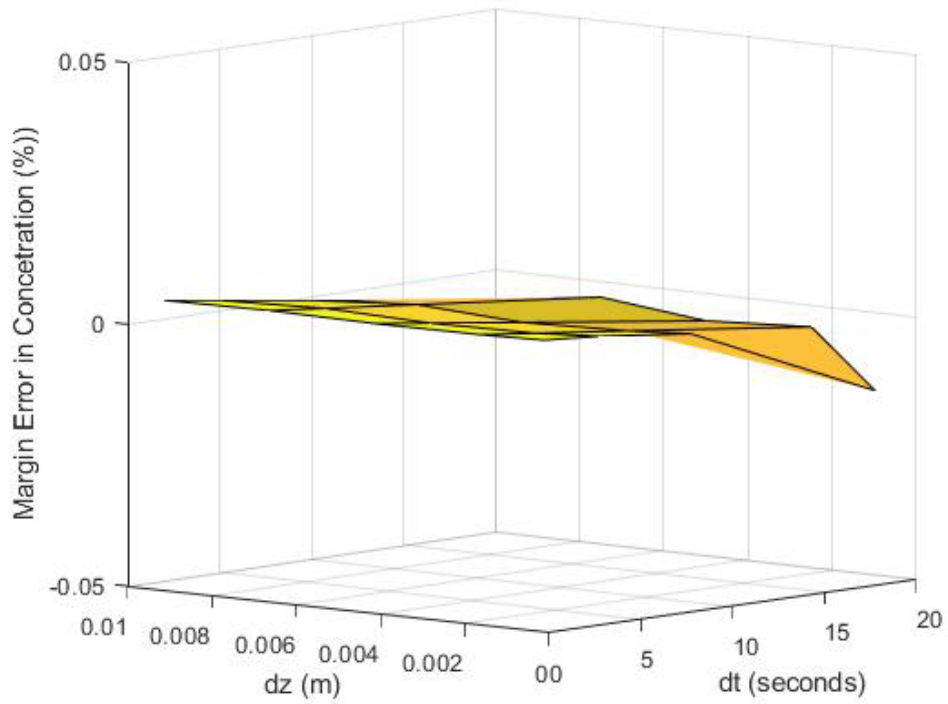
Figure 4.2: 3D plot of sensitivity to the selection of time and space grids (*dt* and *dz*).

4.4.2 Coupled Transport Model for PFAS

A MATLAB script ("*m.file*") was developed using the forward and central finite-difference methods for time and space, respectively, to couple the simulations of the transport of PFAS and seepage. The seepage and transport models were one-way coupled to simulate the overall PFAS Transport as impacted by seepage. In this case, the one-way coupling was made possible using coupled parameters of flow velocity (v) and volumetric water content (θ). Using the seepage model, the velocities and volumetric water contents were computed for every node at every time using the seepage model and imported into the PFAS transport model, thereby, creating a one-way coupled simulation of the transport of PFAS in both vadose and saturated zones. Below are different scenarios resulting from each independent model and the above-mentioned coupling.

4.4.3 Seepage Model Testing and Analysis

First, the two models were tested using cases with well-known flow fields.

(a)   (b)
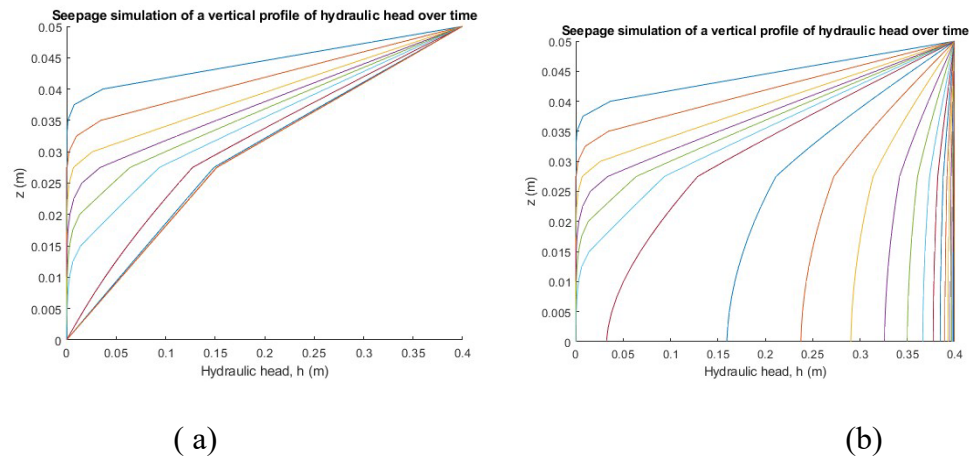
Figure 4.3: The vertical profile of the seepage flow with (a) locked seepage and (b) unlocked seepage.

Figure 4.3 shows the vertical profiles of the hydraulic head at different time steps 10-second apart for two cases. Both cases of Figure 4.3 have a constant head at the top inlet

(H_1 = 0.4 m). The difference is in the total head boundary condition at the outlet. Figure 4.3(a) shows a case where a contact head H_2 = 0 m is maintained at the bottom outlet—referred to as the 'locked case' modeled using a Dirichlet boundary condition—while Figure 4.3(b) shows the case where the total head H_2 at the bottom outlet is allowed to increase—referred to as 'unlocked case' using a Newman boundary condition.

(a)   (b)
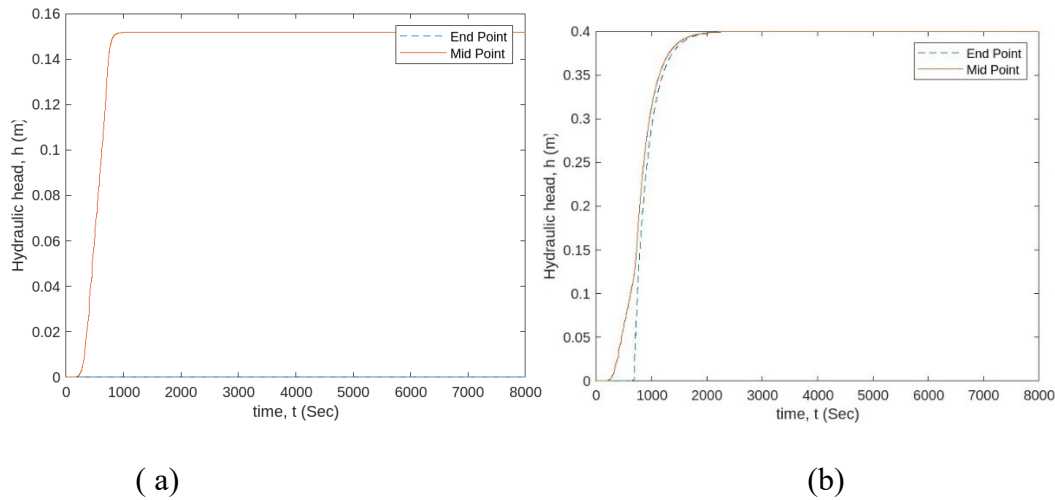
Figure 4.4: Time history for seepage for the outlet as (a) locked and (b) unlocked

Figure 4.4 shows the time history of the cases of Figure 4.3. As seen, Figures 4.4(a) and 4.4(b) each show the time history at two different points, the mid-point and at the outlet. The dashed red line represents the mid-point results while the dashed blue line represents the end point. As mentioned, the hydraulic head is maintained constant at zero for the locked case and is allowed to increase (until equilibrium is reached) for the unlocked case, respectively. In Figure 4.4(a), the total head at the outlet remains zero while the midpoint grows slowly. On the other hand, Figure 4.4(b) shows that the hydraulic head at both the outlet and midpoint grows to reach equilibrium (i.e., equal with the inlet value), which is consistent with the set boundary conditions.

4.4.4 PFAS Transport

The transport of PFAS in the same domain was also simulated using the parameters mentioned in Section 4.3.1. Figure 4.5 shows the vertical profile of concentration at various times 10-second intervals apart for two types of boundary conditions. The first, shown in Figure 4.5(a), is for a constant input concentration of a contaminant at the inlet (top) equal to 12 mg/L and an infinite body of fresh water at the outlet (bottom), where the concentration remains 0 mg/L and is not accumulated—referred to as locked. The second case, Figure 4.5(b), shows the vertical profile over time for a constant feed of 12 mg/L at the inlet (top) and a small body of water that allows the accumulation of the contaminant and increase in its concentration at the outlet (bottom)—referred to as unlocked—until equilibrium is reached. In this case, diffusion and advection are simulated without adsorption terms.

(a)   (b)
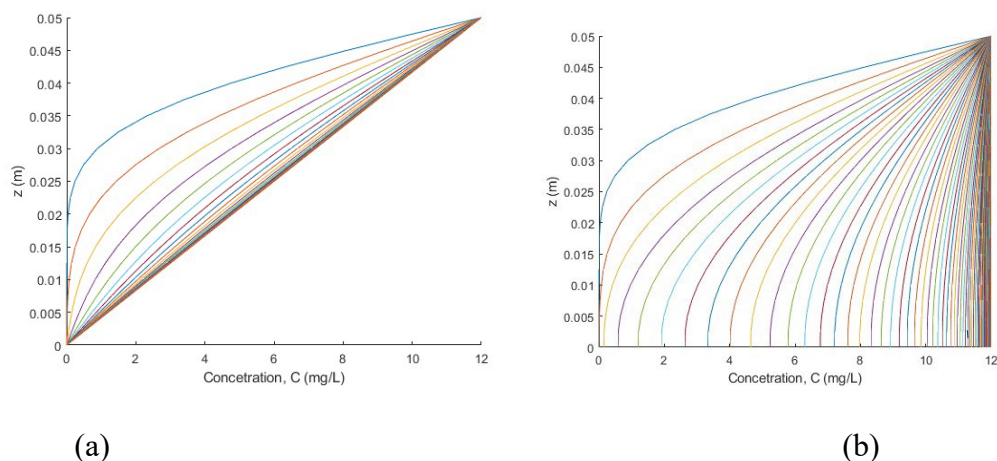
Figure 4.5. Vertical Profile over time of concentration for: (a) constant feed at the top and fresh water at the bottom and (b) a constant feed at the top and breakthrough at the bottom, shown at time increment of 10 seconds

(a)   (b)
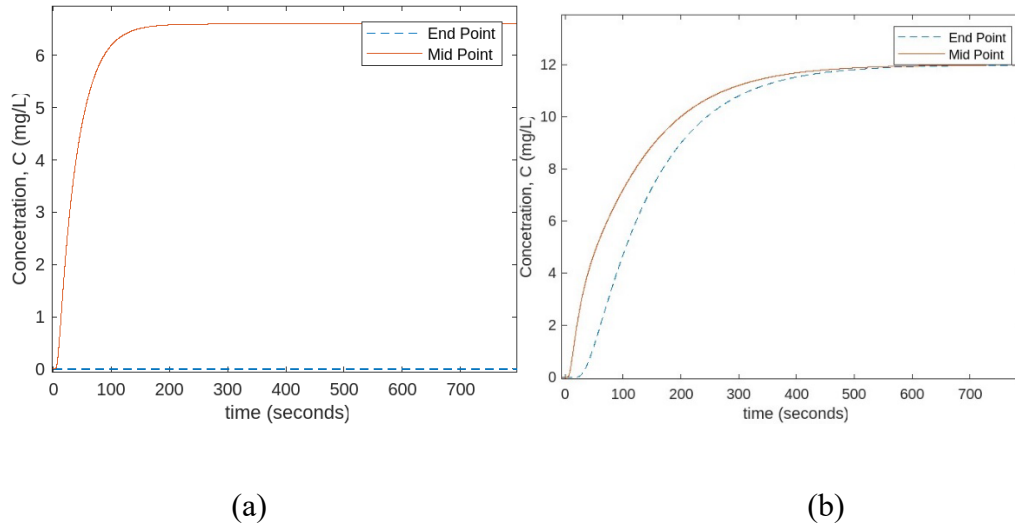
Figure 4.6: The breakthrough curves for (a) constant feed at the top and fresh water at the bottom; and (b) a constant feed at the top and breakthrough at the bottom

Figure 4.6 shows the breakthrough curves of Figures 4.5(a) and 4.5(b). The dashed

red line represents the mid-point case while the dashed blue line represents the endpoint.

4.4.5   Effect of Adsorption coefficients on the transport of PFAS

(a)   (b)
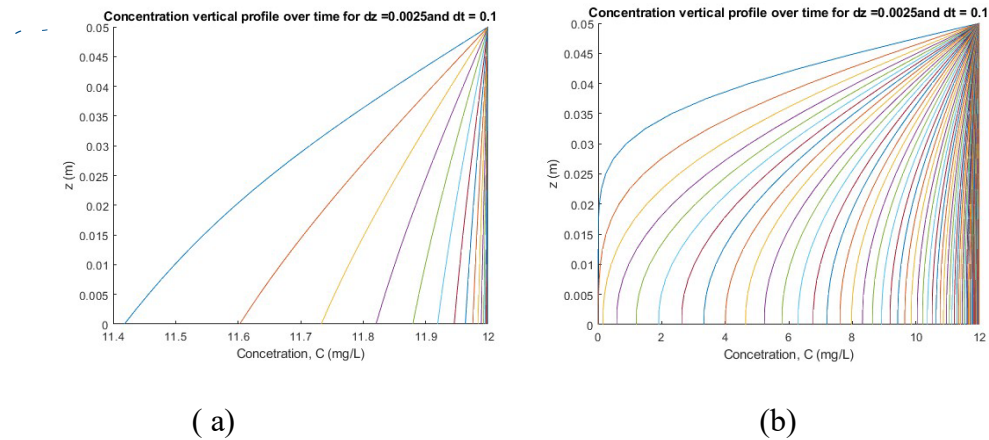
Figure 4.7: Vertical profile of PFAS transport with advection and diffusion and (a) no PFAS adsorption to a solid phase, hence, no retardation; (b) PFAS adsorption to solid particles and retardation

Figure 4.7 is used to show the effect of adsorption to solid particles on the

transport of PFAS for the case with locked outlet boundary condition. Figure 4.7(a)

shows the transport of PFAS before considering the adsorption to solids, and Figure

4.7(b) shows a similar case with adsorption to solid particles considered. It is noteworthy

that in both cases, the degree of water saturation is 100% (no air and air-water interface);

hence, there is no adsorption to the air-water interfaces.

4.3. Impact of degree of Saturation, S_w, on Transport Model

<div align="center">(a)</div>
<div align="center">(b)</div>
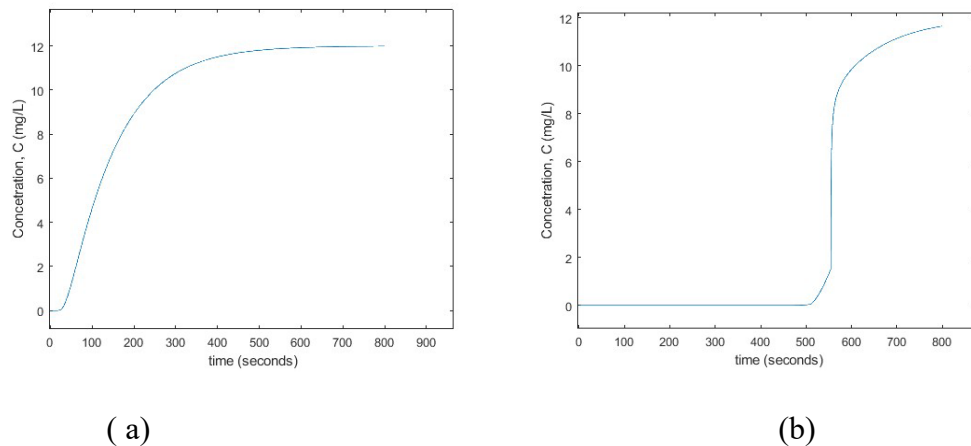
Figure 4.8: Time history of PFAS transport with advection and diffusion: (a) soil is fully saturated, i.e., no air-water interfaces and hence no PFAS adsorption to the interfaces; (b) soil starts from dry and gradually saturates, i.e., there are air-water interfaces and PFAS adsorption to those interfaces

Figure 4.8 is used to show the impact of PFAS micelles formation absorbed on air-water interfaces, retarding PFAS transport. This is evaluated using a change in the degree of water saturation within the PFAS transport model. In other words, the seepage flow model is once run assuming an initial condition with fully water-saturated soil (i.e., no air). Then, the same case is studied using an initial condition with the soil starting off dry and gradually saturating; hence, there will be air and air-water interfaces. Figure 4.8(a) shows the PFAS transport in a fully saturated environment with no air, air-water interfaces, and, hence, no PFAS adsorption to those interfaces, eliminating the corresponding retardation.

Figure 4.8(b) considers the scenario where the soil is initially dry and gradually saturated; hence, there are air, air-water interfaces, and PFAS adsorption to those interfaces and corresponding retardation. At high hydraulic conductivity, the saturation time is short, and the retardation may not be visible at the considered *dt* resolution. However, at low hydraulic conductivity, the impact of the gradual increase in the degree of saturation and the air existence are more pronounced. Figure 4.8(a) shows how concentration moves fast through the saturated soil. On the other hand, Figure 4.8(b) shows that when the soil starts off dry, it takes a much longer time for the PFAS concentration to move through the soil due to the existence of air and PFAS adsorption onto the air-water interfaces. Comparing Figures 4.8(b) and 4.8(a), it is seen that the slope of the breakthrough for the case with air-water interfaces is steeper, i.e., the breakthrough is slower.

4.4. Impact of Hydraulic Conductivity, *k*, on PFAS Transport Model

(a) (b)
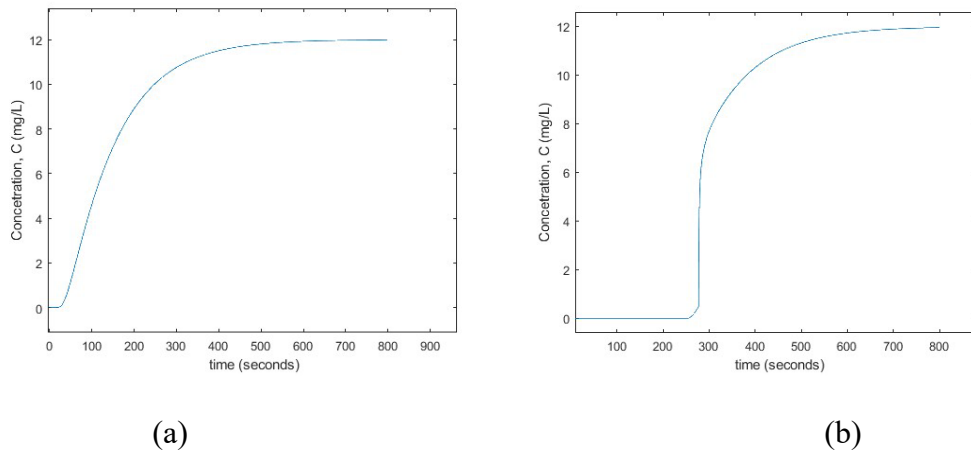
Figure 4.9: Time history of PFAS transport through soils with (a) higher hydraulic conductivity; and (b) lower hydraulic conductivity

Figure 4.9 shows the impact of hydraulic conductivity on the seepage and hence FPAS transport model. The hydraulic conductivity of Figure 4.9(a) is larger than that of

Figure 4.9(b). As expected, both figures show how the PFAS concentration moves through the soil at different paces. The higher hydraulic conductivity corresponds to a faster PFAS transport and shorter breakthrough. Figure 4.9(b) also shows that the slope of the slower breakthrough for the case with lower hydraulic conductivity is steeper.

4.5. Conclusion

PFAS have specific characteristics making them attractive for various applications and products, which has resulted in their widespread use and, in turn, presence in soil and groundwater media. PFAS are mobile and resistant to degradation and can, hence, stay within the environment for a long time. Therefore, understanding their fate and transport in the soil/water environment is paramount to the detection of and developing effective remediation methods for the treatment and removal of these compounds.

This paper covered the development of a numerical model within the MATLAB interface for a 1D transient Transport of PFAS in a soil/water environment. The paper evaluates the effects of various transport processes (advection, diffusion, and adsorption to various phases) on the fate of PFAS within soil and groundwater. After the model was developed, an analysis was carried out to determine whether the selection of the spatial and temporal discretization grid resolution (i.e., selection of time steps, dt, and space grid size, dz) can alter the model results. The results show very minimal (less than 2% of sensitivity) impact by dt and dz within a large range of time and space grid resolutions. Then, using dt and dz where results are not impacted by the choice of discretization grid, multiple scenarios were investigated using the numerical model to understand the fate and transport of PFAS in both vadose and saturated zones in order to qualitatively test and analyze the

results. This model is still being improved to account for more complex scenarios such as biotransformation and co-contamination, which do not fit within the scope of this paper. The 2D version of the model has been developed and is under testing and verification, while the 3D version of the model is still under development. Neither the 2D nor the 3D models fit within the scope of this paper. All input properties were obtained from controlled experiments within the literature; however, the model needs to ultimately be validated using experimental results, which are also ongoing. In terms of future work, there is a need for more research into the role of co-contaminants on the transport of PFAS in the vadose zone. In addition, more research is needed on a wider range of PFAS chain compounds.

4.6. Reference

Araujo, J.B., Mainhagu, J., and Brusseau, M. L. (2015). "Measuring air-water interfacial area for soils using the mass balance surfactant-tracer method." *Chemosphere*, 134, 199–202

Barzen-Hanson, K.A., Roberts, S.C., Choyke, S., Oetjen, K., McAlees, A., Riddell, N., McCrindle, R., Ferguson, P.L., Higgins, C.P., Field, J.A., (2017). "Discovery of 40 classes of per- and polyfluoroalkyl substances in historical aqueous film-forming foams (AFFF) and AFFF-impacted groundwater." *Environ. Sci. Technol.* 51,2047-2057.

Blake, B. E., & Fenton, S. E. (2020). Early life exposure to per- and polyfluoroalkyl substances (PFAS) and latent health outcomes: A review including the placenta as a target tissue and possible driver of peri- and postnatal effects. *Toxicology*, *443*(August), 152565. https://doi.org/10.1016/j.tox.2020.152565

Brusseau, M. L. (2019a). "Estimating the relative magnitudes of adsorption to solid-water and air/oil-water interfaces for per- and poly-fluoroalkyl substances." *Environmental Pollution*, *254*, 113102.

Brusseau, M. L. (2019b). "The influence of molecular structure on the adsorption of PFAS to fluid-fluid interfaces: Using QSPR to predict interfacial adsorption coefficients." *Water Research*, *152*, 148–158.

Brusseau, M. L., Peng, S., Schnaar, G., and Murao, A. (2007). "Measuring air-water interfacial areas with X-ray microtomography and interfacial partitioning tracer tests." *Environmental Science & Technology*, 41(6), 1956–1961

Brusseau, Mark L., Van Glubt, Sarah, 2019. "The influence of surfactant and solution composition on PFAS adsorption at fluid-fluid interfaces." *Water Res.* 161, 17–26.

Buck RC, Franklin J, Berger U, Conder JM, Cousins IT, De Voogt P, Jensen AA, Kannan K, Mabury, SA, and Van Leeuwen SP (2011). "Perfluoroalkyl and Polyfluoroalkyl Substances in the Environment: Terminology, Classification, and Origins." *Integrated environmental assessment and management*. 7:4:513. [PubMed: 21793199]

Ding, G., & Peijnenburg, W. (2013). Physicochemical Properties and Aquatic Toxicity of Poly- and Perfluorinated Compounds. *Critical Reviews in Environmental Science And Technology*, *43*(6), 598-678. doi: 10.1080/10643389.2011.627016

Fredlund, D. G., (1997). "Soil Mechanics for unsaturated soils." *China Architecture & Building Press*, Beijing Shi, China.

Guo, Bo & Zeng, Jicai and Brusseau, Mark. (2020). "A Mathematical Model for the Release, Transport, and Retention of Per- and Polyfluoroalkyl Substances (PFAS) in the Vadose Zone." *Water Resources Research*. 56. 10.1029/2019WR026667

Houtz, E. F., Higgins, C. P., Field, J. A., & Sedlak, D. L. (2013). "Persistence of perfluoroalkyl acid precursors in AFFF-impacted groundwater and soil." *Environmental Science and Technology*, *47*(15), 8187–8195. https://doi.org/10.1021/es4018877

Jordan Jr., Ernest David. (1981). "A modified Crank-Nicolson Method." *Master Thesis, Virginian Commonwealth University*. https://doi.org/10.25772/WAV4-6029

Kim, H., Rao, P. S. C., and Annable, M. D. (1997). "Determination of effective air-water interfacial area in partially saturated porous media using surfactant adsorption." *Water Resources Research*, *33*(12), 2705–2711.

Li, Y., Oliver, D., & Kookana, R. (2018). A critical analysis of published data to discern the role of soil and sediment properties in determining sorption of per and polyfluoroalkyl substances (PFASs). *Science Of the Total Environment*, *628-629*, 110-120. https://doi.org/10.1016/j.scitotenv.2018.01.167

Liew, Z., Goudarzi, H. & Oulhote, Y. (2018). "Developmental Exposures to Perfluoroalkyl Substances (PFASs): An Update of Associated Health Outcomes." *Curr Envir Health Rpt* **5,** 1–19. https://doi.org/10.1007/s40572-018-0173-4

Lyu Y., Brusseau M.L., Chen, W., Yan, N., Fu, X., and Lin, X. (2018). "Adsorption of PFOA at the Air-Water Interface during Transport in Unsaturated Porous Media." *Environ Sci Technol*. 2018 Jul 17 ;52(14) :7745-7753. DOI : 10.1021/acs.est.8b02348. E-pub, Jun 26. PMID: 29944343; PMCID: PMC6312111.

Nian, M., Luo, K., Luo, F., Aimuzi, R., Huo, X., Chen, Q., Tian, Y., & Zhang, J. (2020). "Association between Prenatal Exposure to PFAS and Fetal Sex Hormones: Are the Short-Chain PFAS Safer." *Environmental Science and Technology*, *54*(13), 8291–8299. https://doi.org/10.1021/acs.est.0c02444

Sharifan, Hamidreza, Bagheri, Majid, Wang, Dan, Burken, Joel G., Higgins, Christopher P., Liang, Yanna, Liu, Jinxia, Schaefer, Charles E., and Blotevogel, Jens, (2021). "Fate and transport of per- and polyfluoroalkyl substances (PFASs) in the vadose zone." Science of the total environment, Volume 771, 145427.

Schaefer, C., Drennan, D. M., Tran, D. N., Garcia, R., Christie, E., Higgins, C. P., and Field, J. A. (2019). "Measurement of aqueous diffusivities for perfluoroalkyl acids." *Journal of Environmental Engineering*, 145(11), 06019006.

Steenland, K., Kugathasan, S., & Barr, D. B. (2018). "PFOA and ulcerative colitis." *Environmental Research*, *165*(May), 317–321. https://doi.org/10.1016/j.envres.2018.05.007

Vieira, V. M., Hoffman, K., Shin, H. M., Weinberg, J. M., Webster, T. F., & Fletcher, T. (2013). "Perfluorooctanoic acid exposure and cancer outcomes in a contaminated community: a geographic analysis." *Environmental health perspectives*, *121*(3), 318–323. https://doi.org/10.1289/ehp.1205829

Wang, Zhanyun, DeWitt, Jamie C., Higgins, Christopher P., and Cousins, Ian T., (2017)." A never-ending story of per-and polyfluoroalkyl substances (PFAS)." *Environ. Sci. Technol*. 51,2508-6623.

Xu, Y., Li, Y., Scott, K., Lindh, C. H., Jakobsson, K., Fletcher, T., Ohlsson, B., & Andersson, E. M. (2020). "Inflammatory bowel disease and biomarkers of gut inflammation and permeability in a community with high exposure to

perfluoroalkyl substances through drinking water." *Environmental Research*, *181*(November 2019), 108923. https://doi.org/10.1016/j.envres.2019.108923

Xu, M., & Eckstein, Y. (1995). "Use of weighted least-squares method in the evaluation of the relationship between dispersity and field scale." Groundwater, 33(6), 905–908.

62

CHAPTER FIVE: Conclusions

This research investigated the fate and transport of PFAS in vadose and saturated

zones of soils. The study was conducted through one-way coupling of two numerical

models. First, a transient seepage model was developed and used to simulate the

hydraulic head and flow velocity in both vadose and saturated environments. Then a

PFAS transport model was developed taking into consideration various factors governing

PFAS transport behavior, i.e., molecular diffusion, advection, mechanical dispersion, and

adsorption to solids and to air-water interfaces. The two models were one-way coupled in

order to investigate the fate and transport of PFAS within the vadose zones, i.e., flow

velocity and volumetric water content results are found at each time and location nodes

using the seepage model and input into the PFAS model to find PFAS concentration at

each time and location nodes. After the two models were developed and coupled, the

impact of the choice of the spatial and time discretization grids' resolution (i.e., selection

of time steps, dt, and space grid size, dz) on the simulation results were studied to find a

range of dt and dz that results in the same results. Lastly, the models were used to

simulate different scenarios and qualitatively analyze and test the effects of adsorption

coefficients, hydraulic conductivity, and degree of water-saturation on the PFAS

transport. Major findings from this study are listed below.

- The transport of PFAS was simulated using a combination of the seepage flow
  with the PFAS transport processes (advection, molecular diffusion,
  mechanical dispersion, adsorption to solid phase and adsorption to air-water
  interfaces).

- Various boundary conditions can be simulated to maintain constant to allow an increase in the hydraulic head and PFAS concentration on boundaries. For example, for the seepage model, the total heads at the inlet and outlet can be locked to remain constant to simulate constant-head tests, or the hydraulic head at the outlet can be allowed to raise.

- The developed models' results are impacted by the choice of time and space grid discretization over a reasonably large range of dz and dt.

- The models are able to capture the effects of molecular diffusion, advection, mechanical dispersion, coefficients of adsorption to solid and air-water interfaces, degree of water- and air-saturation, and hydraulic conductivity on the transport of PFAS. A retardation of PFAS transport was observed when adsorption coefficients were introduced into the model. The change in the degree of water saturation within the PFAS transport model—i.e., introduction of air content—indirectly leads to adsorption to air-water interfaces and micelles formation.

Future Research:

There are several phenomena that could be considered for further improvement of the model. Some future research recommendations could include the following.

- 2D and 3D versions of the model are needed for more complex flow geometry.

- Experimental validation is still needed for the model.

- Most current research focusses on PFOS and PFOA, more research is still needed for a wider range of PFAS compounds.

- The model only considers the presence of PFAS in soils. Research is needed to investigate the role co-contaminants could have on the transport of PFAS.

APPENDIX A: DERIVATIONS

1D Transient Seepage Equations

$$\vec{\nabla} \cdot v = -\frac{\partial \theta}{\partial t}$$

$$\frac{\partial \theta}{\partial t} = m_V \frac{\partial h}{\partial t}$$

$$\frac{\partial}{\partial z}\left(-k_z \frac{dh}{dz}\right) = -m_V \frac{\partial h}{\partial t}$$

$$\frac{\partial k}{\partial z}\frac{\partial h}{\partial z} + k \frac{\partial^2 h}{\partial z^2} = m_V \frac{\partial h}{\partial t}$$

$$\frac{k_{ii+1} + k_{ii}}{dz} \cdot \frac{h_{ii+i}^{t^{k+1}} - h_{ii}^{t^{k+1}}}{dz} + k_{ii}\frac{h_{ii+1} - 2h_{ii} + h_{ii-1}}{\Delta z^2} = m_v \frac{h_{ii}^{t^{k+1}} - h_{ii}^{t^{k}}}{\Delta t}$$

$$\frac{k_{ii+1}}{dz^2} h_{ii+1}^{t^{k+1}} - \frac{k_{ii+1}}{dz^2} h_{ii}^{t^{k+1}} - \frac{k_{ii}}{dz^2} h_{ii+1}^{t^{k+1}} + \frac{k_{ii}}{dz^2} h_{ii}^{t^{k+1}} + \frac{k_{ii}}{\Delta z^2} h_{ii+1}^{t^{k+1}} - 2\frac{k_{ii}}{\Delta z^2} h_{ii}^{t^{k+1}}$$

$$+ \frac{k_{ii}}{\Delta z^2} h_{ii-1}^{t^{k+1}} = \frac{m_v h_{ii}^{t^{k+1}}}{dt} - \frac{m_v h_{ii}^{t^{k}}}{dt}$$

$$h_{ii+1}^{t^{k+1}}\left(\frac{k_{ii+1}}{dz^2}\right) + h_{ii}^{t^{k+1}}\left(\frac{-k_{ii+1}}{dz^2} - \frac{k_{ii}}{dz^2} - \frac{m_v}{dt}\right) + h_{ii-1}^{t^{k+1}}\left(\frac{k_{ii}}{dz^2}\right) = -\frac{m_v h_{ii}^{t^{k}}}{dt}$$

$$a(ii, ii+1) = \frac{k_{ii+1}}{dz^2}$$

$$a(ii, ii) = \frac{-k_{ii+1}}{dz^2} - \frac{k_{ii}}{dz^2} - \frac{m_v}{dt}$$

$$a(ii, ii-1) = \frac{k_{ii}}{dz^2}$$

$$b(ii) = -\frac{m_v h_{ii}^{t^{k+1}}}{dt}$$

Diffusion Equation

$$\frac{\partial(\theta C)}{\partial t} = \frac{\partial}{\partial z}\left(\theta D \frac{\partial C}{\partial z}\right)$$

$$\theta \frac{\partial C}{\partial t} + C \frac{\partial \theta}{\partial t} = D \frac{\partial \theta}{\partial z}\frac{\partial C}{\partial z} + \theta \frac{\partial D}{\partial z}\frac{\partial C}{\partial z} + \theta D \frac{\partial^2 C}{\partial z}$$

$$\frac{\partial \theta}{\partial z} D \frac{\partial C}{\partial z} + \frac{\partial D}{\partial z}\theta \frac{\partial C}{\partial z} + \theta D \frac{\partial^2 C}{\partial z} = \frac{\partial \theta}{\partial t} C + \theta \frac{\partial C}{\partial t}$$

$$\frac{\theta_{i+1} - \theta_i}{dz} D_i \frac{C_{i+1}^{t^{k+1}} - C_i^{t^{k+1}}}{dz} + \theta_i \frac{D_{i+1} - D_i}{dz}\frac{C_{i+1}^{t^{k+1}} - C_i^{t^{k+1}}}{dz}$$

$$+ \theta_i D_i \frac{C_{i+1}^{t^{k+1}} - 2C_i^{t^{k+1}} + C_{i-1}^{t^{k+1}}}{dz^2} = \frac{\theta_i^{t^{k+1}} - \theta_i^{t^k}}{dt} C_i + \frac{C_i^{t^{k+1}} - C_i^{t^k}}{dt}\theta_i$$

For

$$C_i = \frac{C_i^{t^{k+1}} + C_i^{t^k}}{2}$$

$$C_{i+1}^{t^{k+1}}\left(D_i \frac{\theta_{i+1}}{dz^2} - D_i \frac{\theta_i}{dz^2} + \theta_i \frac{D_{i+1}}{dz^2} - \theta_i \frac{D_i}{dz^2} + \theta_i \frac{D_i}{dz^2} - C_i^{t^{k+1}}\left(D_i \frac{\theta_{i+1}}{dz^2} - D_i \frac{\theta_i}{dz^2}\right.\right.$$

$$+ \theta_i \frac{D_{i+1}}{dz^2} - \theta_i \frac{D_i}{dz^2} + 2\frac{\theta_i D_i}{dz^2} + \frac{\theta_i^{t^{k+1}} - \theta_i^{t^k}}{dt} + \frac{\theta_i}{dt}\right)$$

$$= C_i^{t^k}\left(\frac{\theta_i^{t^{k+1}}}{2dt} - \frac{\theta_i^{t^k}}{2dt} - \frac{\theta_i}{dt}\right)$$

$$C_{i+1}^{t^{k+1}}\left(\frac{D_i \theta_{i+1}}{dz^2} + \frac{\theta_i D_{i+1}}{dz^2} - \frac{D_i \theta_i}{dz^2}\right) - C_i^{t^{k+1}}\left(\frac{D_i \theta_{i+1}}{dz^2} + \frac{\theta_i D_{i+1}}{dz^2} + \frac{\theta_i}{dt} + \frac{\theta_i^{t^{k+1}} - \theta_i^{t^k}}{2dt}\right)$$

$$+ C_{i-1}^{t^{k+1}}\left(\frac{\theta_i D_i}{dz^2}\right) = C_i^{t^k}\left(\frac{\theta_i^{t^{k+1}}}{2dt} - \frac{\theta_i^{t^k}}{2dt} - \frac{\theta_i}{dt}\right)$$

Advection Equation

$$\frac{\partial}{\partial t} = \frac{\partial}{\partial z}(\theta v C)$$

$$\frac{\partial}{\partial z}(\theta v C) = \frac{\partial(\theta C)}{\partial t}$$

$$-vc\frac{\partial \theta}{\partial z} - \theta C \frac{\partial v}{\partial z} - \theta v \frac{\partial C}{\partial z} = \frac{\partial(\theta C)}{\partial t}$$

$$-v_i C_i \frac{\theta_{i+1}^{t^{k+1}} - \theta_i^{t^{k+1}}}{dz} - \theta_i C_i \frac{v_{i+1}^{t^{k+1}} - v_i^{t^{k+1}}}{dz} - \theta_i v_i \frac{C_{i+1}^{t^{k+1}} - C_i^{t^{k+1}}}{dz} = \theta \frac{dC}{dt} + C \frac{d\theta}{dt}$$

$$-\frac{v_i \theta_{i+1}^{t^{k+1}}}{dz} C_i + \frac{v_i \theta_i^{t^{k+1}}}{dz} C_i - \frac{\theta_i v_{i+1}^{t^{k+1}}}{dz} C_i + \frac{\theta_i v_i^{t^{k+1}}}{dz} C_i - \frac{\theta_i v_i}{dz} C_{i+1}^{t^{k+1}} + \frac{\theta_i v_i}{dz} C_i^{t^{k+1}}$$

$$= \frac{\theta_i^{t^{k+1}} - \theta_i^{t^k}}{dt} C_i + \frac{C_i^{t^{k+1}} - C_i^{t^k}}{dt} \theta_i$$

$$C_i \left(-\frac{v_i \theta_{i+1}^{t^{k+1}}}{dz} + \frac{v_i \theta_i^{t^{k+1}}}{dz} - \frac{\theta_i v_{i+1}^{t^{k+1}}}{dz} + \frac{\theta_i v_i^{t^{k+1}}}{dz} \right) - \frac{\theta_i v_i}{dz} C_{i+1}^{t^{k+1}} + \frac{\theta_i v_i}{dz} C_i^{t^{k+1}}$$

$$= \frac{\theta_i^{t^{k+1}} - \theta_i^{t^k}}{dt} C_i + \frac{C_i^{t^{k+1}} - C_i^{t^k}}{dt} \theta_i$$

For

$$C_i = \frac{C_i^{t^{k+1}} + C_i^{t^k}}{2}$$

$$C_i^{t^{k+1}}\left(-\frac{v_i\theta_{i+1}^{t^{k+1}}}{2dz}+\frac{v_i\theta_i^{t^{k+1}}}{2dz}-\frac{\theta_i v_{i+1}^{t^{k+1}}}{2dz}+\frac{\theta_i v_i^{t^{k+1}}}{2dz}+\frac{\theta_i v_i}{dz}-\frac{\theta_i}{dt}-\frac{\theta_i^{t^{k+1}}-\theta_i^{t^k}}{2dt}\right)$$

$$-\frac{\theta_i v_i}{dz}C_{i+1}^{t^{k+1}}$$

$$=C_i^{t^k}\left(-\frac{v_i\theta_{i+1}^{t^{k+1}}}{2dz}+\frac{v_i\theta_i^{t^{k+1}}}{2dz}-\frac{\theta_i v_{i+1}^{t^{k+1}}}{2dz}+\frac{\theta_i v_i^{t^{k+1}}}{2dz}\right)+C_i^{t^k}(\frac{\theta_i^{t^{k+1}}}{2dt}-\frac{\theta_i^{t^k}}{2dt}$$

$$-\frac{\theta_i}{dt})$$

$$C_i^{t^{k+1}}\left(-\frac{v_i\theta_{i+1}^{t^{k+1}}}{2dz}+\frac{v_i\theta_i^{t^{k+1}}}{2dz}-\frac{\theta_i v_{i+1}^{t^{k+1}}}{2dz}+\frac{\theta_i v_i^{t^{k+1}}}{2dz}+\frac{\theta_i v_i}{dz}-\frac{\theta_i}{dt}-\frac{\theta_i^{t^{k+1}}-\theta_i^{t^k}}{2dt}\right)$$

$$-C_{i+1}^{t^{k+1}}\left(\frac{\theta_i v_i}{dz}\right)$$

$$=-C_i^{t^k}(-\frac{v_i\theta_{i+1}^{t^{k+1}}}{2dz}+\frac{v_i\theta_i^{t^{k+1}}}{2dz}-\frac{\theta_i v_{i+1}^{t^{k+1}}}{2dz}+\frac{\theta_i v_i^{t^{k+1}}}{2dz}-\frac{\theta_i^{t^{k+1}}}{2dt}+\frac{\theta_i^{t^k}}{2dt}+\frac{\theta_i}{dt})$$

Advection - Diffusion:

$$C_{i+1}^{t^{k+1}}\left(\frac{D_i\theta_{i+1}}{dz^2}+\frac{\theta_i D_{i+1}}{dz^2}-\frac{D_i\theta_i}{dz^2}-\frac{\theta_i v_i}{dz}\right)-C_i^{t^{k+1}}\left(\frac{D_i\theta_{i+1}}{dz^2}+\frac{\theta_i D_{i+1}}{dz^2}+\frac{\theta_i}{dt}+\frac{\theta_i^{t^{k+1}}-\theta_i^{t^k}}{2dt}\right)$$

$$+\frac{v_i\theta_{i+1}^{t^{k+1}}}{2dz}-\frac{v_i\theta_i^{t^{k+1}}}{2dz}+\frac{\theta_i v_{i+1}^{t^{k+1}}}{2dz}-\frac{\theta_i v_i^{t^{k+1}}}{2dz}-\frac{\theta_i v_i}{dz}\right)+C_{i-1}^{t^{k+1}}\left(\frac{\theta_i D_i}{dz^2}\right)$$

$$=-C_i^{t^k}(-\frac{\theta_i^{t^{k+1}}}{2dt}+\frac{\theta_i^{t^k}}{2dt}+\frac{\theta_i}{dt}-\frac{v_i\theta_{i+1}^{t^{k+1}}}{2dz}+\frac{v_i\theta_i^{t^{k+1}}}{2dz}-\frac{\theta_i v_{i+1}^{t^{k+1}}}{2dz}+\frac{\theta_i v_i^{t^{k+1}}}{2dz})$$

$$\theta_i=\frac{\theta_i^{t^{k+1}}+\theta_i^{t^k}}{2}$$

$$D_i = \frac{D_i^{t^{k+1}} + D_i^{t^k}}{2}$$

Solid Phase Adsorption

$$\frac{\partial(\theta C)}{\partial t} = -\rho_b k_f \frac{\partial}{\partial t} C^N$$

$$-\rho_b k_f \frac{\partial}{\partial t} C^N = \frac{\partial(\theta C)}{\partial t}$$

$$-\rho_b k_f N C^{N-1} \frac{\partial C}{\partial t} = \frac{\partial(\theta C)}{\partial t}$$

Let $-\rho_b k_f N C^{N-1}$=F

$$-F \frac{\partial C}{\partial t} = \theta \frac{\partial C}{\partial t} + C \frac{\partial \theta}{\partial t}$$

$$-F \left(\frac{C_i^{t^{k+1}} - C_i^{t^k}}{dt} \right) = \frac{\theta_i^{t^{k+1}} - \theta_i^{t^k}}{dt} C_i + \frac{C_i^{t^{k+1}} - C_i^{t^k}}{dt} \theta_i$$

$$-\frac{F C_i^{t^{k+1}}}{dt} + \frac{F C_i^{t^k}}{dt} = C_i^{t^{k+1}} \left(\frac{\theta_i}{dt} + \frac{\theta_i^{t^{k+1}}}{2dt} + \frac{-\theta_i^{t^k}}{2dt} \right) + C_i^{t^k} \left(\frac{\theta_i^{t^{k+1}}}{2dt} - \frac{\theta_i^{t^k}}{2dt} - \frac{\theta_i}{dt} \right)$$

Air -Water Adsorption

$$\frac{\partial(\theta C)}{\partial t} = -\frac{\partial}{\partial t}(A_{aw} k_{a\omega} C)$$

$$-\frac{\partial}{vt}(A_{aw} k_{a\omega} C) = \frac{\partial(\theta C)}{\partial t}$$

$$-\left(k_{a\omega}C\frac{\partial A_{aw}}{\partial t}+A_{aw}C\frac{\partial}{\partial t}+A_{aw}k_{a\omega}\frac{\partial C}{\partial t}\right)=\theta\frac{\partial C}{\partial t}+C\frac{\partial \theta}{\partial t}$$

$$-\left[k_{a\omega_i}C_i\left(\frac{A_{aw_i}^{t^{k+1}}-A_{aw_i}^{t^k}}{dt}\right)+A_{aw_i}C_i\left(\frac{k_{aw_i}^{t^{k+1}}-k_{aw_i}^{t^k}}{dt}\right)\right.$$

$$\left.+A_{aw_i}k_{aw_i}\left(\frac{C_i^{t^{k+1}}-C_i^{t^k}}{dt}\right)\right]=\frac{\theta_i^{t^{k+1}}-\theta_i^{t^k}}{dt}C_i+\frac{C_i^{t^{k+1}}-C_i^{t^k}}{dt}\theta_i$$

$$-k_{a\omega_i}C_i\left(\frac{A_{aw_i}^{t^{k+1}}}{dt}\right)+k_{a\omega_i}C_i\left(\frac{A_{aw_i}^{t^k}}{dt}\right)-A_{aw_i}C_i\left(\frac{k_{aw_i}^{t^{k+1}}}{dt}\right)+A_{aw_i}C_i\left(\frac{k_{aw_i}^{t^k}}{dt}\right)$$

$$+A_{aw_i}k_{aw_i}\left(\frac{C_i^{t^{k+1}}}{dt}\right)-A_{aw_i}k_{aw_i}\left(\frac{C_i^{t^k}}{dt}\right)$$

$$=C_i^{t^{k+1}}\left(\frac{\theta_i}{dt}+\frac{\theta_i^{t^{k+1}}}{2dt}+\frac{-\theta_i^{t^k}}{2dt}\right)+C_i^{t^k}(\frac{\theta_i^{t^{k+1}}}{2dt}-\frac{\theta_i^{t^k}}{2dt}-\frac{\theta_i}{dt})$$

For

$$C_i=\frac{C_i^{t^{k+1}}+C_i^{t^k}}{2}$$

$$-k_{a\omega_i}\left(\frac{A_{aw_i}^{t^{k+1}}}{dt}\right)(\frac{C_i^{t^{k+1}}+C_i^{t^k}}{2})+k_{a\omega_i}\left(\frac{A_{aw_i}^{t^k}}{dt}\right)(\frac{C_i^{t^{k+1}}+C_i^{t^k}}{2})$$

$$-A_{aw_i}\left(\frac{k_{aw_i}^{t^{k+1}}}{dt}\right)(\frac{C_i^{t^{k+1}}+C_i^{t^k}}{2})+A_{aw_i}\left(\frac{k_{aw_i}^{t^k}}{dt}\right)(\frac{C_i^{t^{k+1}}+C_i^{t^k}}{2})$$

$$+A_{aw_i}k_{aw_i}\left(\frac{C_i^{t^{k+1}}}{dt}\right)-A_{aw_i}k_{aw_i}\left(\frac{C_i^{t^k}}{dt}\right)$$

$$=C_i^{t^{k+1}}\left(\frac{\theta_i}{dt}+\frac{\theta_i^{t^{k+1}}}{2dt}+\frac{-\theta_i^{t^k}}{2dt}\right)+C_i^{t^k}(\frac{\theta_i^{t^{k+1}}}{2dt}-\frac{\theta_i^{t^k}}{2dt}-\frac{\theta_i}{dt})$$

$$-k_{a\omega_i} \frac{A_{aw_i}^{t^{k+1}}}{dt} \frac{C_i^{t^{k+1}}}{2} - k_{a\omega_i} \frac{A_{aw_i}^{t^{k+1}}}{dt} \frac{C_i^{t^k}}{2} + k_{a\omega_i} \frac{A_{aw_i}^{t^k}}{dt} \frac{C_i^{t^{k+1}}}{2} + k_{a\omega_i} \frac{A_{aw_i}^{t^k}}{dt} \frac{C_i^{t^k}}{2}$$

$$- A_{aw_i} \frac{k_{aw_i}^{t^{k+1}}}{dt} \frac{C_i^{t^{k+1}}}{2} - A_{aw_i} \frac{k_{aw_i}^{t^{k+1}}}{dt} \frac{C_i^{t^k}}{2} + A_{aw_i} \frac{k_{aw_i}^{t^k}}{dt} \frac{C_i^{t^{k+1}}}{2}$$

$$+ A_{aw_i} \frac{k_{aw_i}^{t^k}}{dt} \frac{C_i^{t^k}}{2} + A_{aw_i} k_{aw_i} \frac{C_i^{t^{k+1}}}{dt} - A_{aw_i} k_{aw_i} \frac{C_i^{t^k}}{dt}$$

$$= C_i^{t^{k+1}} \left(\frac{\theta_i}{dt} + \frac{\theta_i^{t^{k+1}}}{2dt} + \frac{-\theta_i^{t^k}}{2dt} \right) + C_i^{t^k} \left(\frac{\theta_i^{t^{k+1}}}{2dt} - \frac{\theta_i^{t^k}}{2dt} - \frac{\theta_i}{dt} \right)$$

$$C_i^{t^{k+1}} \left(-k_{a\omega_i} \frac{A_{aw_i}^{t^{k+1}}}{2dt} + k_{a\omega_i} \frac{A_{aw_i}^{t^k}}{2dt} - A_{aw_i} \frac{k_{aw_i}^{t^{k+1}}}{2dt} + A_{aw_i} \frac{k_{aw_i}^{t^k}}{2dt} + \frac{A_{aw_i} k_{aw_i}}{dt} \right)$$

$$+ C_i^{t^k} \left(-k_{a\omega_i} \frac{A_{aw_i}^{t^{k+1}}}{2dt} + k_{a\omega_i} \frac{A_{aw_i}^{t^k}}{2dt} - A_{aw_i} \frac{k_{aw_i}^{t^{k+1}}}{2dt} + A_{aw_i} \frac{k_{aw_i}^{t^k}}{2dt} \right.$$

$$\left. - \frac{A_{aw_i} k_{aw_i}}{dt} \right) = C_i^{t^{k+1}} \left(\frac{\theta_i}{dt} + \frac{\theta_i^{t^{k+1}}}{2dt} + \frac{-\theta_i^{t^k}}{2dt} \right) + C_i^{t^k} \left(\frac{\theta_i^{t^{k+1}}}{2dt} - \frac{\theta_i^{t^k}}{2dt} - \frac{\theta_i}{dt} \right)$$

APPENDIX B: MATLAB CODES

M. File in MATLAB to Numerically calculate the Hydraulic Head (Transient

Seepage)

```matlab
clc; close all;
gw=9.806;

h1=0.40; h2=0;
dz=0.0025;%dz=0.5
L=0.05;%L=5;
m=floor(L/dz)+1;% number of nodes
p=floor(m/2);

a=zeros(m,m); a=a*0;
ac=zeros(m,m); ac=ac*0;

b=1:m; b=b*0; %zeros(m);
x=0:dz:(m-1)*dz;
z=(L-x)';

dt=0.1;
tfinal=800; %sec

nt=fix(tfinal/dt); % time steps

frac =0.5;
k0zz2=0.015e-7*0.5;
k0zz1=frac*k0zz2;

for ii=1:p
    k0zz(ii)=k0zz1;
end
for ii=(p+1):m
    k0zz(ii)=k0zz2;
end

a1=1;
a2=3;
h0=0; h0(1)=h1; h0(m)=h2;

hold=z*0;
hold(1)=h1; hold(m)=h2;
h=hold;
ht=zeros(m,nt);
ht(:,1)=hold;
sw=zeros(m,nt); sw(2:m,1)=0;sw(1,1)=1;
```

```matlab
phi(1:m,1:nt)=0.00294; theta=phi.*sw;
kzz=k0zz./(1+a1*abs(hold-z).^a2); %initial hydraulic conductivity

%new hydraulic conductivity
kzold=0;

figure;
hold on;

%Time steps
for tt=1:nt-1
   kzold=kzold*0.5; %TO force the while loop at the beginning of
each time step
    %While loop within each step to update parameters
    while abs(max(kzz-kzold))/k0zz1>0.001 % can use K0zz1 or
k0zz2

        %Boundary Condition at point 1

        a(1,:)=0;
        a(1,1)=1;

        ac(1,:)=0;
        ac(1,1)=1;

        b(1)=h1;
        %Boundary Condition at point m
        a(m,:)=0;
        a(m,m)=1;

        ac(m,:)=0;
        ac(m,m)=1;

        b(m)=h2;

        %General Core Equations Coefficients
        for ii=2:(m-1)

            if (h(ii)-z(ii))>=0
                mv=0.00001; mvi(ii)=mv;% for Saturated soils
                kzz(ii)=k0zz(ii);
            else
                kzz(ii)=k0zz(ii)/(1+a1*abs((h(ii)+hold(ii))/2-
z(ii)).^a2);
                mv=0.0005; mvi(ii)=mv;% for unsaturated soils
            end
```

```matlab
        a(ii, ii)=-(kzz(ii+1)+kzz(ii))/dz^2-(mv/dt);

        a(ii,ii-1)=(kzz(ii)/dz^2);

        a(ii,ii+1)=(kzz(ii+1)/dz^2);


        b(ii)=-mv/dt*hold(ii);
    end

    %SOlving AX=B
    h=a^-1*b';

    %update Parameter based on (h+hold)/2) central difference
method
    kzold=kzz;

    for jj=1:m

        if (h(jj)-z(jj))>=0
            kzz(jj)=k0zz(jj);
        else

            kzz(jj)=k0zz(jj)./(1+a1*abs((h(jj)+hold(jj))/2-
z(jj)).^a2);   %updating hydraulic conductivity
        end

        %     kzz-kzold
    end

end % end of While loop

%Ready to go to the next time
hold=h;
ht(:,tt+1)=h; % h stored

plot(h,z) % plotting h,z
if h(m)~h2;
    disp('error');
end

for ii=1:m-1

    theta(:,tt+1)=theta(:,tt)+mvi(ii)*(ht(:,tt+1)-ht(:,tt));
```

```
        sw(:,tt+1)=theta(:,tt+1)./phi(:,tt+1);
        if (h(ii)-z(ii))>=0
            sw(ii,tt)=1;
            theta(ii,tt)=phi(ii,tt)*sw(ii,tt);
        else

        end
        v(ii,tt)=-kzz(ii)*(ht(ii+1,tt)-ht(ii,tt))/dz;
        v(ii,tt+1)=-kzz(ii)*(ht(ii+1,tt+1)-ht(ii,tt+1))/dz;

    end
    v(m,tt)=v(m-1,tt);
    v(m,tt+1)=v(m-1,tt);

end
xlabel('Hydraulic head, h (m)');ylabel('z (m)')
title('Seepage simulation of a vertical profile of hydraulic head
over time');

figure;
plot(1:nt,ht(m,:))
xlabel('time (sec)');ylabel('Hydraulic head, h (m)')
```

M. File in MATLAB to Simulate the Transport of PFAS in the vadose saturated

zones

```
%clear all;
```

```matlab
clc; close all;
gw=9.806;

kf=0.5;    %fitting parameter for solid-phase adsorption
N=0.85;  %fitting parameter for solid-phase adsorption
dens=1.65; %density g/cm3
x0=633.96; %fitting parameter   for Aaw
x1=-1182.5; %fitting parameter    for Aaw
x2=548.58; %fitting parameter    for Aaw
gamma0=0.071; % Surface tension in dyn/m
p=4*10^-5; % fitting parameter
q=0.107; % fitting Parameter
R=8.314; %gas constant
T=293.15; %Constant temperature
% dzi=[0.001,0.0025,
0.005,0.0075,0.01];%0.005;%[0.0001,0.0005,0.001,0.005,0.01];%0.00
05:0.00025:0.01;%[0.0025,0.005,0.01];%,0.005,0.01,0.05,0.1,0.5];
% dti=[2,5,10,20];%20;%[0.2,1,2,10,20];%100:50:2000;
%];%,0.2,1,2,10,20];
dzi=0.0025;
dti=0.1;
cond=input('Boundary condition (0 for Constant zero at outlet and
1 for varying concentration = ');

sas=input('Is there additional adsorption to solids (O for No, 1
for Yes) = ');
saa=input('Is there additional adsorption to air (O for No, 1 for
Yes) = ');
L=0.05;%      in m %
tfinal=800; %sec

mv=1; %Retention capacity for unsaturated soils
frac =1;
D02=0.15e-2;%5.4e-6 m/sec
D01=frac*D02;



for idz=1:length(dzi)
   dz=dzi(idz);
for idt=1:length(dti)
   dt=dti(idt);
%dz=0.005;% in m %
%dt=20;   %sec
```

```matlab
m=floor(L/dz)+1;% number of nodes
p=floor(m/2);

a=zeros(m); %a=a*0;

b=1:m; b=b*0; %zeros(m);
x=0:dz:(m-1)*dz;
z=(L-x)';

%dt=20;
nt=fix(tfinal/dt); % time steps
ttplot=zeros(nt,1);
Ct=zeros(m,nt);
C=zeros(m,1);
%zz1=3e-4; %Initial guess for hydraulic conductivity


for ii=1:p
    D0(ii,1:nt)=D01;
end
for ii=(p+1):m
    D0(ii,1:nt)=D02;
end

%Comment this out for coupling too **************
% sw(1:m,1:nt)=0.5;
% phi(1:m,1:nt)=0.00294; theta0=phi.*sw;
% theta=theta0;
%********************

Aaw=(x2.*sw.^2+x1.*sw+x0); %Air-water interfacial Area

Cold=zeros(1,m); %Cold=Cold*0.0000; %zeros(m,1);
C1=12; C2_0=0.000001;
Cold(1)=C1; Cold(m)=C2_0;
Ct=zeros(m,nt); % c stored
Ctzt=zeros(m,nt,length(dzi),length(dti));
Ct(:,1)=Cold;
Ctzt(:,1,idz,idt)=Cold;


C=Cold;
C2=C2_0;

Kaw=zeros(m,nt);
F=zeros(m,1);
```

```matlab
atest=1;
Kaw0(:,1)=atest*gamma0*q./(R*T*(p+Cold)); % initial air-water
interfacial adsorption coefficient

F0(:,1)=kf*dens*N*(Cold+1e-10*ones(1,m)).^(N-1);     %%initial F
parameter
% v needs to be commented out for coupling to use v from
transient
% Seepage*****************
% v(1:m,1:nt)=0.015e-7*0.5; %velocity (m/s)
%***************************

Dcn(1:m)=0; % Diffusion coefficient
thetacn(1:m)=0; % volumetric content
vcn(1:m)=0;    % velocity
Fcn(1:m,1)=0;    %F  Cranck-Nicolson
Kawcn(1:m,1)=0; % Air-water adsorption coefficient Cranck-
Nicolson
Aawcn(1:m,1)=0; % Air-water Interfacial area Cranck-Nicolson


figure;
hold on;

Ct(:,1)=Cold; % h stored

%Time steps
for tt=1:nt-1
    %disp(tt);

    D=D0;%*(1+a1*(C.^a2));  %new hydraulic conductivity

   F(:)=1.1*F0(:);
   cc=max(abs(Kaw0))+.001;
   dd=max(abs(F0))+.001;

   counter=0;

   while (max(abs(F(:)-F0(:)))/dd>0.001 || max(abs(Kaw(:,tt+1)-
Kaw0(:)))/cc>0.001)  && counter<10000

       if max(abs(F(:)-F0(:)))>10000
           disp('erorr in F = ');
       end
       if max(abs(Kaw(:,tt+1)-Kaw0(:)))>10000
```

```matlab
            disp('erorr in Kaw = ');
        end

        counter=counter+1;


        for jj=1:m
            Dcn(jj)=(D(jj,tt+1)+D(jj,tt))/2;   % D Cranck-Nicolson
            thetacn(jj)=(theta(jj,tt+1)+theta(jj,tt))/2; %theta
Cranck-Nicolson
            vcn(jj)=(v(jj,tt+1)+v(jj,tt))/2; % v crank-nicolson

Kawcn(jj)=gamma0*q./(R*T*(p+(Ct(jj,tt)+Ct(jj,tt+1))/2)); %
initial air-water interfacial adsorption coefficient
            Fcn(jj)=kf*dens*N*((Ct(jj,tt)+Ct(jj,tt+1))/2+1e-
10).^(N-1);    %%initial F parameter
        end


%Boundary Condition at Point 1

        a(1,:)=0;
        a(1,1)=1;

        b(1)=C1;

    %Boundary Condition at point m

        a(m,:)=0;
        a(m,m)=1;

        b(m)=C2;

    %General Core Equations Coefficients
        for ii=2:(m-1)


            % With diffusion & Advection
            a(ii,ii)=-
(Dcn(ii+1)*thetacn(ii)+Dcn(ii)*thetacn(ii+1))/dz^2-
thetacn(ii)*1/dt+(theta(ii,tt+1)-theta(ii,tt))/2/dt-
((theta(ii+1,tt+1)*vcn(ii)+theta(ii,tt)*vcn(ii)-
thetacn(ii)*v(ii+1,tt+1)+thetacn(ii)*v(ii,tt))/2*dz)+thetacn(ii)*
vcn(ii)/dz;%-(mv/dt);
            %With Solid-Phase Adsorption
            if sas==1
```

```matlab
                a(ii,ii)= a(ii,ii)-(Fcn(ii)/dt);
            end
            %With  Air-water Interface adsorption
            if saa==1
                a(ii,ii)= a(ii,ii)-
((Kawcn(ii)*Aaw(ii,tt+1)/2*dt)+(Kawcn(ii)*Aaw(ii,tt+1)/2*dt)-
(Aawcn(ii)*Kaw(ii,tt+1)/2*dt)+(Aawcn(ii)*Kaw(ii,tt)/2*dt)-
(Aawcn(ii)*Kawcn(ii)/dt));
            end



            % With Advection
            a(ii,ii-1)=thetacn(ii)*Dcn(ii)/dz^2;
            %With Solid-Phase Adsorption
            %a(ii,ii-1)=a(ii,ii-1);
            %With Air-water Interface adsorption
            %a(ii,ii-1)=a(ii,ii-1);


            % With Advection

a(ii,ii+1)=(thetacn(ii)*Dcn(ii+1)+thetacn(ii+1)*Dcn(ii)-
thetacn(ii)*Dcn(ii))/dz^2-thetacn(ii)*vcn(ii)/dz;
            %With Solid-Phase Adsorption
            %a(ii,ii+1)=a(ii,ii+1);
            %With Air-water Interface adsorption
            %a(ii,ii+1)=a(ii,ii+1)

            %with Advection
            b(ii)=-mv*Cold(ii)*((-
theta(ii,tt+1)/2+theta(ii,tt)/2+thetacn(ii))/dt-
(theta(ii+1,tt+1)*vcn(ii)+theta(ii,tt+1)*vcn(ii)-
(thetacn(ii)*v(ii+1,tt+1)+thetacn(ii)*v(ii,tt+1))/2*dz));
            %With Solid-Phase Adsorption
            if sas==1
                b(ii)=b(ii)-(mv*Cold(ii)*(Fcn(ii)/dt));
            end
            %With Air-water Interface adsorption
            if saa==1
                b(ii)=b(ii)-
mv*Cold(ii)*((Kawcn(ii)*Aaw(ii,tt+1)/2*dt)-
(Kawcn(ii)*Aaw(ii,tt)/2*dt)+(Aawcn(ii)*Kaw(ii,tt+1)/2*dt)-
(Aawcn(ii)*Kaw(ii,tt)/2*dt)-(Aawcn(ii)*Kawcn(ii)/dt));
            end
```

```matlab
        end % end of space loop

        %SOlving AX=B
        C=a^-1*b';
        C(m);
        Ct(:,tt+1)=C; % h stored

         %Updating parameters

        Kaw0(:)=Kaw(:,tt+1);
        F0=F;

        for jj=1:m

            Kaw(jj,tt+1)=atest*gamma0*q/(R*T*(p+Ct(jj,tt+1)));

            F(jj)=kf*N*dens*(Ct(jj,tt+1)+1e-10)^(N-1);

        end

end    % end of while loop


    %Ready to go to the next time
    Cold=C;

    Ct(:,tt+1)=C; % h stored
     %Cztdzdt(:,tt+1,idz,idt)=C;

%    % ***The following can be commented out for plotting
purposes********
  if rem(tt,100)==0
     plot(C,z); % plotting c,z
  end
%      %**********************************************


    if C(m)~=C2
        disp('error');
    end

    if cond==0
        C2=0;
    elseif cond==1
        C2=C(m-1);
    end
```

```matlab
end %end of time loop
%
%  % ***The following can be commented out for plotting
purposes********
%title(['Concentration vertical profile over time for dz
=',num2str(dz),'and dt = ',num2str(dt)]);
xlabel('Concetration, C (mg/L)');ylabel('z (m)');


hold off;

%***The following can be commented out for plotting
purposes********

% % Breakthrough ****
ttplot=dt*(1:nt);izspec=floor((length(z))/2);itspec=floor(nt/2);
%figure; plot(ttplot,Ct(m,:));%figure; plot(ttplot,Ct(izspec,:));

figure; plot(ttplot,Ct(m,:),'--',ttplot,Ct(floor(m/2),:),'-
');legend('End Point','Mid Point');
xlabel('time, t (Sec)');ylabel('Concetration, C (mg/L))')


 %title(['Breakthrough Curve for z = ',num2str(z(izspec)), ' for
dz =',num2str(dz),'and dt = ',num2str(dt)]);
ylabel('Concetration, C (mg/L)');xlabel(' time (seconds)');
%**************************************************


%Wrong Cdzdt(idz,idt)=Cztdzdt(izspec,itsepc,idz,idt);
Cdzdt(idz,idt)=Ct(izspec,itspec);

clear a; clear b; clear C; clear Ct; clear Cold; clear ttplot;
clear theta; clear thetacn; clear theta0;
clear F; clear F0; clear Fcn; clear z; clear D0; clear Dcn; clear
phi; clear sw;
clear Aaw; clear Aawcn; clear Kaw; clear Kaw0; clear Kawcn; clear
v; clear vcn;
end % end for dz
    end % end for dt

% %Sensitivity Analysis for specific dt and all dz *****
% zspec=floor(max(z)/2); itspec=floor(length(ttplot))/2;
% idtspec=floor(length(dti)/2);
```

```matlab
% figure; plot(dzi,Cdzdt(:,idtspec));
% title(['Concentration at z = ',num2str(L/2), ' for time =
',num2str(tfinal/2),' for all dzs and for dt = ',num2str(dti)]);
% ylabel('Concetration, C (mg/L)');xlabel(' dz (m)');
%
% %Sensitivity Analysis for specific dz and all dt *****
% ttspec=floor(max(ttplot)/2);
% idzspec=floor(length(dzi)/2);
% figure; plot(dti,Cdzdt(idzspec,:));
% title(['Concentration at z = ',num2str(L/2), ' for time =
',num2str(tfinal/2),' for all dts and for dz = ',num2str(dzi)]);
% ylabel('Concetration, C (mg/L)');xlabel(' dt (seconds)');

%Sensitivity Analysis for specific dt and all dz *****
%idtspec=floor(length(dti)/2);
figure; hold on;
for idtspec=1:length(dti)
    plot(dzi,Cdzdt(:,idtspec));
end
title(['Concentration at z = ',num2str(L/2), ' for time =
',num2str(tfinal/2),' for all dzs and for dt = ',num2str(dti)]);
ylabel('Concetration, C (mg/L)');xlabel(' dz (m)');
hold off;

figure; hold on;
%Sensitivity Analysis for specific dz and all dt *****
%ttspec=floor(max(ttplot)/2);
%idzspec=floor(length(dzi)/2);
for idzspec=1:length(dzi)
    plot(dti,Cdzdt(idzspec,:));
end
title(['Concentration at z = ',num2str(L/2), ' for time =
',num2str(tfinal/2),' for all dts and for dz = ',num2str(dzi)]);
ylabel('Concetration, C (mg/L)');xlabel(' dt (seconds)');


% pdzdt=meshgrid(dzi,dti); surf(dti,dzi,Cdzdt); axis([0 20 , 0
0.01, 11 13]);
% figure;
% relC=(Cdzdt-mean(mean(Cdzdt)))/mean(mean(Cdzdt));
% pdzdt=meshgrid(dzi,dti); surf(dti,dzi,relC); %axis([0 20 , 0
0.01, 11 12]);
%
%
% surf(dti,dzi,relC);
% axis([0 20 , 0 0.01, 0 0.05])
```

```
% axis([0 20 , 0 0.01, 0 0.005])
% axis([0 20 , 0 0.01, -0.005 0.005])
% axis([0 20 , 0 0.01, -0.05 0.05])
```